Degree in Industrial Technologies

Bachelor's final project

Automatic Cortical Bone Thickness Analysis in Pediatric Tibiae from CT Imaging

Author
Corpas González, María Dolores.

Supervised by
Sánchez Merchante, Luis Francisco.
Jiménez Octavio, Jesús Ramón.

Collaborating entity:
Children's Hospital of Philadelphia

Madrid
July 2025

María Dolores Corpas González, declara bajo su responsabilidad, que el Proyecto con título **Automatic Cortical Bone Thickness Analysis in Pediatric Tibiae from CT Imaging** presentado en la ETS de Ingeniería (ICAI) de la Universidad Pontificia Comillas en el curso académico 2024/25 es de su autoría, original e inédito y no ha sido presentado con anterioridad a otros efectos. El Proyecto no es plagio de otro, ni total ni parcialmente y la información que ha sido tomada de otros documentos está debidamente referenciada.

Fdo.: ..... Fecha: 22 / 07 / 2025

Autoriza la entrega:

El Director del Proyecto

Luis Francisco Sánchez Merchante

2025.07.22
17:05:27
+02'00'

Fdo.: ..... Fecha: ..... / ..... / .....

El Co-Director del proyecto

Jesús Ramón Jiménez Octavio

Jesús R. Jiménez-Octavio 06259224G

Firmado digitalmente por Jesús R. Jiménez-Octavio 06259224G
Fecha: 2025.07.22 17:20:36 +02'00'

Fdo.: ..... Fecha: ..... / ..... / .....

Title: CORTICAL BONE THICKNESS ANALYSIS IN PEDIATRIC TIBIAE FROM CT IMAGING

Author: Corpas González, María Dolores.
Directors: Sánchez Merchante, Luis Francisco; Jiménez Octavio, Jesús Ramón.
Collaborating entity: Children's Hospital of Philadelphia.

ABSTRACT

A statistical evaluation of pediatric cortical bone thickness development with two automated methods—one matrix-based and one profile-based—for measuring from CT scan data is presented. Using a dataset from the Children's Hospital of Philadelphia, measurements of both the whole bone and its central region were analyzed, stratifying results by age and gender to assess developmental trends and methodological agreement using Bland-Altman plots.

A significant systematic disagreement was found when analyzing the whole bone, with the matrix method yielding consistently higher thickness values. The discrepancy was attributed to the matrix method's inclusion of the entire, thicker epiphysis. However, also in the analysis of the 40-60% zone, the results were counterintuitive and incoherent.

Crucially, the profile-based method demonstrated biologically plausible growth patterns, showing, generally, an increase in thickness with age.

In conclusion, this study contributes with a statistical analysis of pediatric bone thickness development, providing quantitative insights into a previously under-documented area. By leveraging a validated automated measurement tool, the developmental trajectory of the tibia in children from 0 to 17 years could be characterized. It also confirms the feasibility of automated pediatric bone analysis and establishes the profile-based approach as a more robust and reliable tool. Its alignment with expected biological trends makes it a promising method for future research and potential clinical applications.

Keywords: Cortical Bone Thickness, Pediatric Bone Development, CT, Thickness Analysis.

Introduction

While the importance of bone health in children is well-recognized, comprehensive statistical data on the developmental trajectory of cortical bone thickness remains limited, especially data derived from automated, objective methods. This gap in normative data presents a challenge for both the clinical assessment of skeletal health and research into musculoskeletal pathologies.

This gap with a two-fold objective is addressed in this project. The primary aim is to conduct a novel statistical analysis of bone development, providing new insights into how bone thickness changes throughout childhood. Secondly, polishing and validating the algorithm provided, and comparing which methodology is better for the bone thickness study.

The validation is achieved by rigorously comparing two distinct outputs from the algorithm: a matrix-based method and a profile-based method. Using a clinical dataset from the Children's Hospital of Philadelphia, the agreement and bias between these approaches across the whole bone and its central region using Bland-Altman analysis is assessed. The statistical study then leverages the validated method to map developmental trends, with results stratified by age and gender.

By validating a reliable automated tool and applying it to generate new developmental data, this project contributes to a deeper, quantitative understanding of pediatric bone growth. The findings are intended to serve as a foundation for future research and as a potential reference for clinical practice, offering a more precise way to monitor skeletal health in children.

Project Definition

The project aims to perform a foundational statistical analysis of pediatric bone growth. The primary objective is to conduct a comprehensive statistical analysis of pediatric tibial cortical bone thickness, characterizing developmental trends across different age groups and genders.
What is more, the improvement and implementation of a pre-existing computational algorithm made by Alberto Sánchez Bonastre [1] to ensure it provides accurate and reliable measurements suitable for a robust statistical study.
To validate it, two outputs (matrix vs profile methods) are compared, ensuring the selection of the most robust method for the main analysis.

Upon completion, this project is expected to deliver the following outcomes:

1. A validated computational pipeline for the automated measurement of pediatric cortical bone thickness.

2. A new reference dataset of normative tibial cortical thickness values for children, providing valuable information on developmental trends.

3. A comprehensive document that details the project's methodology and findings, serving as a resource for future research in pediatric orthopedics and medical imaging.

Model Description

The input data consists of DICOM files, which are processed to extract the bone structure using thresholding and morphological operations. STL files are generated, smoothed, and aligned with a reference bone (an 11-year-old male tibia) to ensure uniform orientation.

Thickness measurements are calculated by analyzing cross-sectional profiles (e.g., Profile 5) and computing Signed Distance Functions between inner and outer cortical surfaces. The measurements are stored in NumPy arrays (matrices) and Pickle files (profiles).

Two distinct methods are employed:

- **Matrix-based method**: Calculates mean thickness from 3D matrices database.

- **Profile-based method**: Measures cortical thickness across defined profile sections.

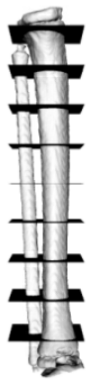

(a) Bone divided into 9 profiles

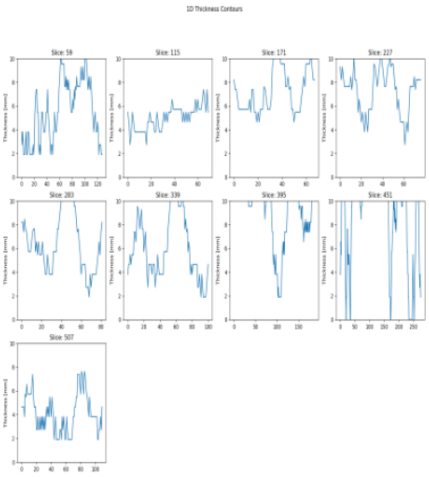

(b) Pickled thickness

Figure 1: Bone profiles and thickness measurements.

The statistical methodology involved two key components. A Bland-Altman analysis was employed to assess the agreement and systematic bias between the matrix and profile methods. Following this comparison, the developmental trajectory of bone thickness was investigated by calculating and plotting the mean and standard deviation for distinct age and gender groups.

Results

The processed dataset includes tibiae from children aged 0 to 17 years. Age groups were divided into five ranges after research. Analysis focused on overall and central average thickness, gender-based trends, and comparison between measurement methods.

Matrix-Based Analysis

Matrix results showed inconsistent trends, with some age ranges exhibiting a decrease in thickness. Possible causes include image resolution, misalignment, or insufficient data. For instance, the following graphic plots the data from the whole bone analysis:

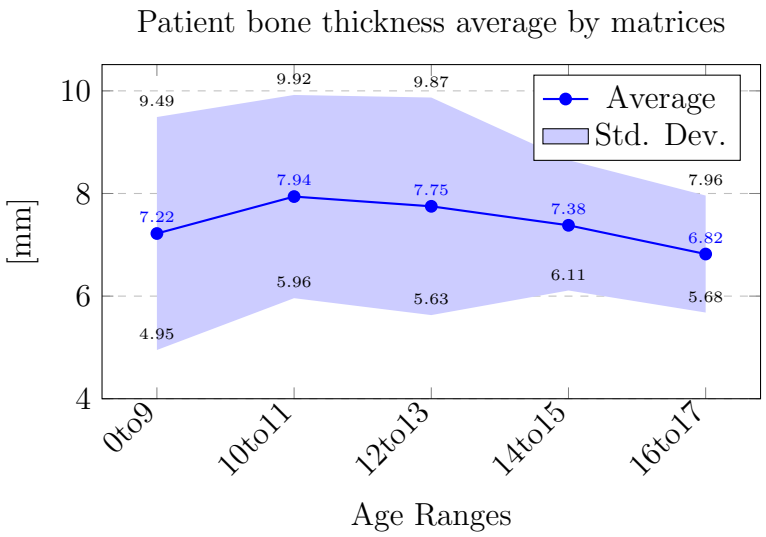

Figure 2: Bones' thickness average with standard deviation.

Profile-Based Analysis

More consistent growth patterns were observed using profile measurements. Cortical thickness increased with age during puberty and stabilized thereafter, aligning with known biological growth phases.

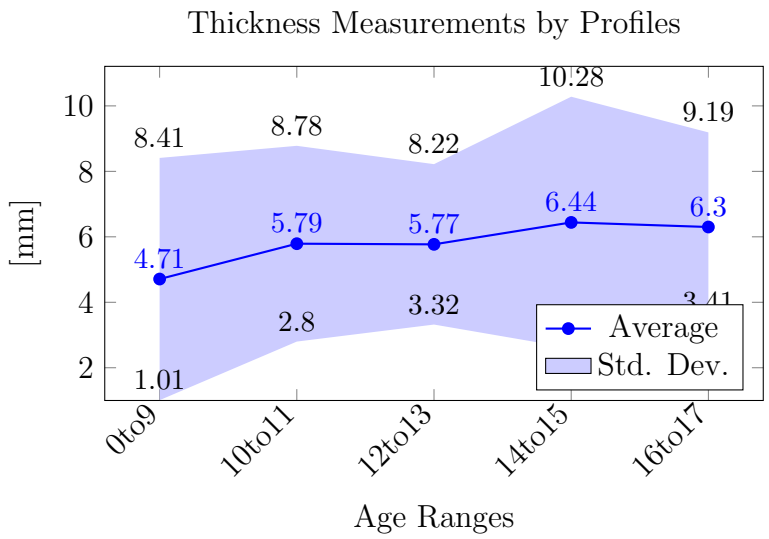

Figure 3: Thickness development by profiles, with standard deviation.

Gender Comparison

Female tibiae showed slower growth as expected, while male samples showed peaks in cortical thickness. These results are consistent with general pediatric growth curves.

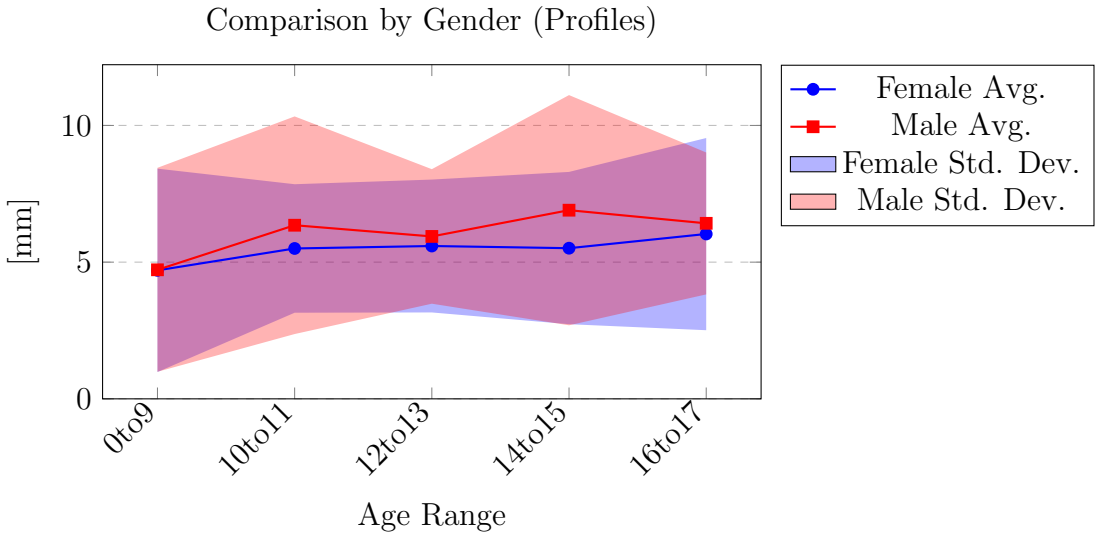

Figure 4: Thickness development by profiles and gender, with standard deviation bands.

Conclusions

The improved algorithm demonstrates the potential for fully automated cortical thickness analysis in pediatric CT imaging. The profile-based method is especially promising, providing accurate and interpretable measurements. However, some results were also counterintuitive and incoherent due to the decrease in bone thickness with age.

Key takeaways include:

- Profile-based methods are more robust than matrix approaches.
- Larger and higher-quality datasets are needed for more definitive conclusions.
- Automation reduces analysis time and human error.
- New statistical data on pediatric bone development, establishing a baseline for future research and clinical applications.

The methodology could be extended in future projects to other long bones, integrated with deep learning models for segmentation, and used for longitudinal studies in pediatric development and disease tracking.

Bibliography

1. Sánchez-Bonaste, Alberto, et al. "Systematic measuring cortical thickness in tibiae for bio-mechanical analysis." *Computers in Biology and Medicine*, vol. 163, 2023, p. 107123.

2. Chudler, Eric H. "Brain Slicing: A Primer on Brain Anatomy." 2023, `https://faculty.washington.edu/chudler/slice.html`. Accessed 19 July 2024.

3. Ağırdil, Yücel. "The growth plate: a physiologic overview." *EFORT open reviews*, vol. 5, no. 8, 2020, pp. 498-507.

4. Chen, Howard. "DICOM Processing and Segmentation in Python." *Radiology Data Quest*, Np 28, 2017.

5. Du, Wenjing, Jinhuan Zhang, and Jingwen Hu. "A method to determine cortical bone thickness of human femur and tibia using clinical CT scans." *2018 IRCOBI conference proceedings, Athens (Greece)*, 2018, pp. 403-412.

6. Perry, R. J., C. Farquharson, and S. F. Ahmed. "The role of sex steroids in controlling pubertal growth." *Clinical endocrinology*, vol. 68, no. 1, 2008, pp. 4-15.

7. Ota, Shingo, et al. "Cortical thickness mapping at segmented regions in the distal radius using HR-pQCT." *Journal of Bone and Mineral Metabolism*, vol. 40, no. 6, 2022, pp. 1021-1032.

8. Nilsson, Ola, et al. "Endocrine regulation of the growth plate." *Hormone research in paediatrics*, vol. 64, no. 4, 2005, pp. 157-165.

9. Murray, Philip G., and Peter E. Clayton. "Endocrine Control of Growth." *American Journal of Medical Genetics Part C: Seminars in Medical Genetics*, 2013.

Título: ANÁLISIS DEL GROSOR DEL HUESO CORTICAL EN TIBIAS PEDIÁTRICAS A PARTIR DE IMÁGENES DE TC

Autora: Corpas González, María Dolores.
Directores: Sánchez Merchante, Luis Francisco; Jiménez Octavio, Jesús Ramón.
Collaborating entity: Children's Hospital of Philadelphia.

RESUMEN DEL PROYECTO

Se presenta una evaluación estadística del desarrollo del grosor del hueso cortical pediátrico con dos métodos automatizados —uno basado en matrices y otro en perfiles— para la medición a partir de datos de tomografías computarizadas (TC). Utilizando un conjunto de datos del Children's Hospital of Philadelphia, se analizaron las mediciones tanto del hueso completo como de su región central, estratificando los resultados por edad y género para evaluar las tendencias de desarrollo y la concordancia metodológica mediante gráficos de Bland-Altman.

Se encontró un desacuerdo sistemático significativo al analizar el hueso completo, donde el método basado en matrices arrojó valores de grosor consistentemente más altos. La discrepancia se atribuyó a la inclusión por parte del método de matrices de la epífisis completa, que es más gruesa. Sin embargo, también en el análisis de la zona del 40-60%, los resultados fueron contraintuitivos e incoherentes.

De manera crucial, el método basado en perfiles demostró patrones de crecimiento biológicamente plausibles, mostrando, generalmente, un aumento del grosor con la edad.

En conclusión, este estudio contribuye con un análisis estadístico del desarrollo del grosor del hueso cortical pediátrico, aportando conocimientos cuantitativos sobre un área previamente poco documentada. Aprovechando una herramienta de medición automatizada y validada, se pudo caracterizar la trayectoria de desarrollo de la tibia en niños de 0 a 17 años. También confirma la viabilidad del análisis óseo pediátrico automatizado y establece el enfoque basado en perfiles como una herramienta más robusta y fiable. Su alineación con las tendencias biológicas esperadas lo convierte en un método prometedor para futuras investigaciones y potenciales aplicaciones clínicas.

Palabras Clave: Grosor del Hueso Cortical, Desarrollo Óseo Pediátrico, TC, Análisis de Grosor.

Introducción

Aunque la importancia de la salud ósea en los niños es bien reconocida, los datos estadísticos completos sobre la trayectoria de desarrollo del grosor del hueso cortical siguen siendo limitados, especialmente los datos derivados de métodos automatizados y objetivos. Este vacío en los datos normativos presenta un desafío tanto para la evaluación clínica de la salud esquelética como para la investigación de patologías musculoesqueléticas.

Este proyecto aborda este vacío con un doble objetivo. El objetivo principal es realizar un análisis estadístico novedoso del desarrollo óseo, proporcionando nuevas perspectivas sobre cómo cambia el grosor del hueso a lo largo de la infancia. En segundo lugar, pulir y validar el algoritmo proporcionado, y comparar qué metodología es mejor para el estudio del grosor óseo.

La validación se logra comparando rigurosamente dos resultados distintos del algoritmo: un método basado en matrices y un método basado en perfiles. Utilizando un conjunto de datos clínicos del Children's Hospital of Philadelphia, se evalúa la concordancia y el sesgo entre estos enfoques en todo el hueso y en su región central mediante el análisis de Bland-Altman. El estudio estadístico aprovecha posteriormente el método validado para mapear las tendencias de desarrollo, con resultados estratificados por edad y género.

Al validar una herramienta automatizada fiable y aplicarla para generar nuevos datos sobre el desarrollo, este proyecto contribuye a una comprensión cuantitativa más profunda del crecimiento óseo pediátrico. Los hallazgos pretenden servir como base para futuras investigaciones y como una posible referencia para la práctica clínica, ofreciendo una forma más precisa de monitorizar la salud esquelética en los niños.

Definición del Proyecto

El proyecto tiene como objetivo realizar un análisis estadístico fundamental del crecimiento óseo pediátrico. El objetivo principal es llevar a cabo un análisis estadístico completo del grosor del hueso cortical tibial pediátrico, caracterizando las tendencias de desarrollo en diferentes grupos de edad y géneros.
Además, se contempla la mejora e implementación de un algoritmo computacional preexistente creado por Alberto Sánchez Bonastre [1] para asegurar que proporcione mediciones precisas y fiables, adecuadas para un estudio estadístico robusto.
Para validarlo, se comparan dos resultados (métodos de matrices vs. perfiles), asegurando la selección del método más robusto para el análisis principal.

Al finalizar, se espera que este proyecto ofrezca los siguientes resultados:

1. Un pipeline computacional validado para la medición automatizada del grosor del hueso cortical pediátrico.

2. Un nuevo conjunto de datos de referencia de valores normativos del grosor cortical tibial en niños, proporcionando información valiosa sobre las tendencias de desarrollo.

3. Un documento completo que detalla la metodología y los hallazgos del proyecto, sirviendo como recurso para futuras investigaciones en ortopedia pediátrica e imagen médica.

Descripción del Modelo

Los datos de entrada consisten en archivos DICOM, que son procesados para extraer la estructura ósea mediante umbralización y operaciones morfológicas. Se generan archivos STL, que son suavizados y alineados con un hueso de referencia (una tibia de un niño de 11 años) para asegurar una orientación uniforme.

Las mediciones de grosor se calculan analizando perfiles transversales (p. ej., Perfil 5) y computando Funciones de Distancia con Signo (SDF) entre las superficies corticales interna y externa. Las mediciones se almacenan en arrays de NumPy (matrices) y archivos Pickle (perfiles).

Se emplean dos métodos distintos:

- **Método basado en matrices**: Calcula el grosor medio a partir de una base de datos de matrices 3D.

- **Método basado en perfiles**: Mide el grosor cortical a través de secciones de perfiles definidas.

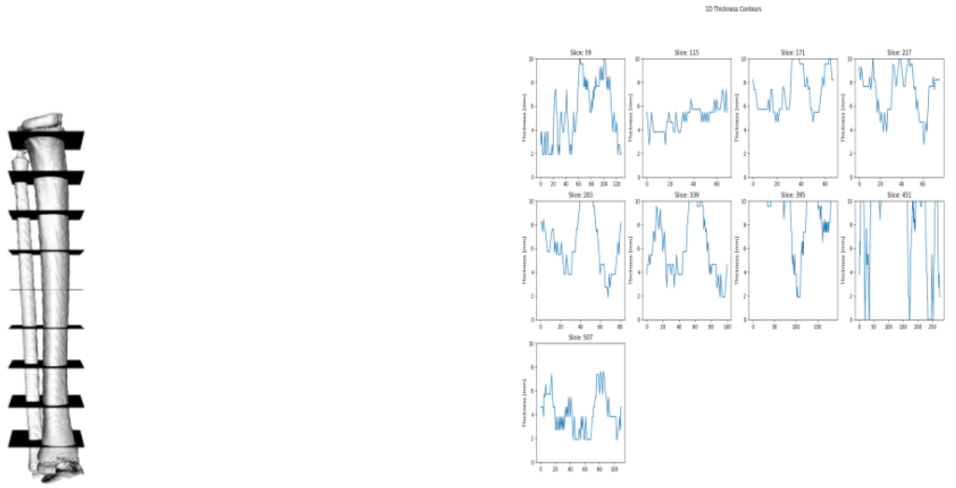

(a) Hueso dividido en 9 perfiles

(b) Grosor de los perfiles (Pickled)

Figure 5: Perfiles óseos y mediciones de grosor.

La metodología estadística implicó dos componentes clave. Se empleó un análisis de Bland-Altman para evaluar la concordancia y el sesgo sistemático entre los métodos de matrices y perfiles. Tras esta comparación, se investigó la trayectoria de desarrollo del grosor óseo calculando y graficando la media y la desviación típica para distintos grupos de edad y género.

Resultados

El conjunto de datos procesado incluye tibias de niños de 0 a 17 años. Los grupos de edad se dividieron en cinco rangos tras una investigación. El análisis se centró en el grosor promedio general y central, las tendencias basadas en el género y la comparación entre los métodos de medición.

Análisis Basado en Matrices

Los resultados de las matrices mostraron tendencias inconsistentes, con algunos rangos de edad exhibiendo una disminución en el grosor. Las posibles causas incluyen la resolución de la imagen, una alineación incorrecta o datos insuficientes. Por ejemplo, el siguiente gráfico muestra los datos del análisis del hueso completo:

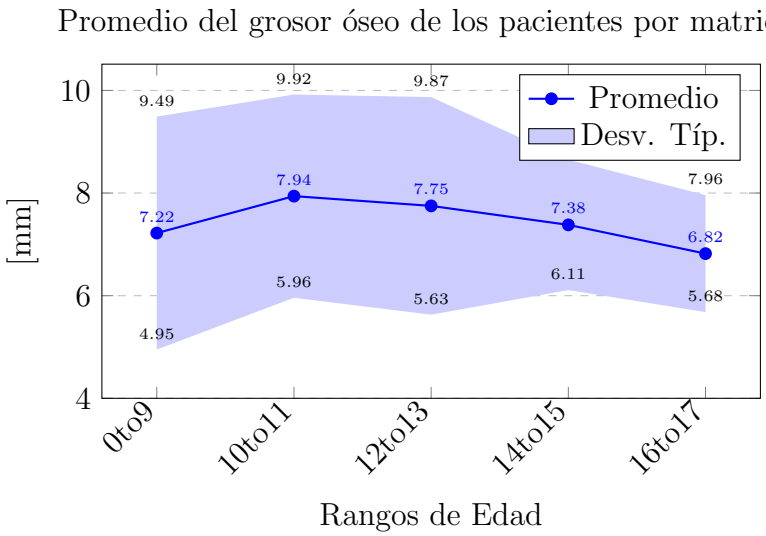

Figure 6: Promedio del grosor de los huesos con desviación típica.

Análisis Basado en Perfiles

Se observaron patrones de crecimiento más consistentes utilizando las mediciones de perfiles. El grosor cortical aumentó con la edad durante la pubertad y se estabilizó después, lo que se alinea con las fases de crecimiento biológico conocidas.

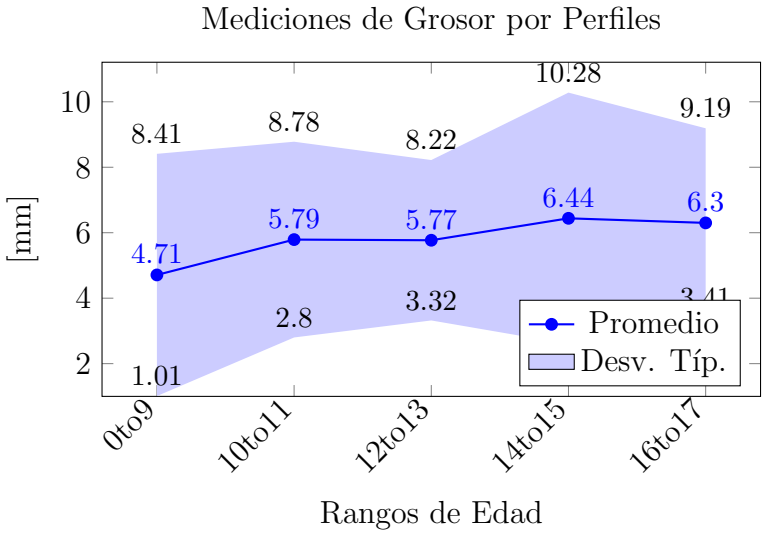

Figure 7: Desarrollo del grosor por perfiles, con desviación típica.

Comparación por Género

Las tibias femeninas mostraron un crecimiento más lento como se esperaba, mientras que las muestras masculinas mostraron picos en el grosor cortical. Estos resultados son consistentes con las curvas generales de crecimiento pediátrico.

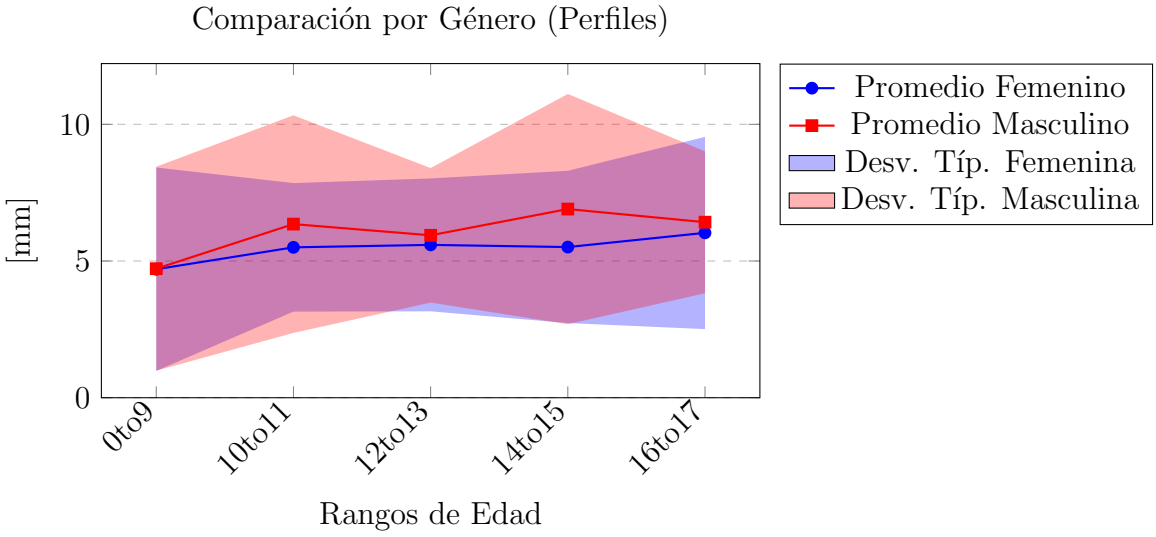

Figure 8: Desarrollo del grosor por perfiles y género, con bandas de desviación típica.

Conclusiones

El algoritmo mejorado demuestra el potencial para un análisis totalmente automatizado del grosor cortical en imágenes de TC pediátricas. El método basado en perfiles es especialmente prometedor, ya que proporciona mediciones precisas e interpretables. Sin embargo, algunos resultados también fueron contraintuitivos e incoherentes debido a la disminución del grosor óseo con la edad.

Las conclusiones clave incluyen:

- Los métodos basados en perfiles son más robustos que los enfoques basados en matrices.
- Se necesitan conjuntos de datos más grandes y de mayor calidad para obtener conclusiones más definitivas.
- La automatización reduce el tiempo de análisis y el error humano.

- Se han obtenido nuevos datos estadísticos sobre el desarrollo óseo pediátrico, estableciendo una base para futuras investigaciones y aplicaciones clínicas.

La metodología podría extenderse en proyectos futuros a otros huesos largos, integrarse con modelos de aprendizaje profundo para la segmentación y utilizarse para estudios longitudinales en el desarrollo pediátrico y el seguimiento de enfermedades.

Bibliografía

1. Sánchez-Bonaste, Alberto, et al. "Systematic measuring cortical thickness in tibiae for bio-mechanical analysis." *Computers in Biology and Medicine*, vol. 163, 2023, p. 107123.

2. Chudler, Eric H. "Brain Slicing: A Primer on Brain Anatomy." 2023, `https://faculty.washington.edu/chudler/slice.html`. Accessed 19 July 2024.

3. Ağırdil, Yücel. "The growth plate: a physiologic overview." *EFORT open reviews*, vol. 5, no. 8, 2020, pp. 498-507.

4. Chen, Howard. "DICOM Processing and Segmentation in Python." *Radiology Data Quest*, Np 28, 2017.

5. Du, Wenjing, Jinhuan Zhang, and Jingwen Hu. "A method to determine cortical bone thickness of human femur and tibia using clinical CT scans." *2018 IRCOBI conference proceedings, Athens (Greece)*, 2018, pp. 403-412.

6. Perry, R. J., C. Farquharson, and S. F. Ahmed. "The role of sex steroids in controlling pubertal growth." *Clinical endocrinology*, vol. 68, no. 1, 2008, pp. 4-15.

7. Ota, Shingo, et al. "Cortical thickness mapping at segmented regions in the distal radius using HR-pQCT." *Journal of Bone and Mineral Metabolism*, vol. 40, no. 6, 2022, pp. 1021-1032.

8. Nilsson, Ola, et al. "Endocrine regulation of the growth plate." *Hormone research in paediatrics*, vol. 64, no. 4, 2005, pp. 157-165.

9. Murray, Philip G., and Peter E. Clayton. "Endocrine Control of Growth." *American Journal of Medical Genetics Part C: Seminars in Medical Genetics*, 2013.

Thank yous

Show special thanks to the Children's Hospital of Philadelphia for providing the data and to my friends from Sweden, Spain and family, who have accompanied me through this period of my life.

Contents

List of Figures

List of Tables

Listings

Chapter 1

Introduction

Medical imaging is a cornerstone of modern healthcare, providing non-invasive windows into the human body that are essential for diagnosis, treatment planning, and monitoring disease. Modalities such as X-ray, Positron Emission Tomography (PET), ultrasound, and Computed Tomography (CT) have revolutionized clinical practice. This project focuses specifically on CT, a powerful method that utilizes computer-processed combinations of many X-ray measurements taken from different angles to produce detailed, cross-sectional 3D images of the body. Compared to traditional 2D radiography, CT offers superior detail and spatial resolution, enabling the detection of subtle fractures, tumours, and other anomalies with much greater clarity.

Despite the high quality of CT scans, a significant challenge remains in translating these rich visual images into objective, quantitative data. Currently, the process of extracting specific measurements—such as the thickness of a particular tissue—is often a manual and laborious task. Radiologists or researchers must use specialized DICOM *(Digital Imaging and Communications in Medicine)* viewers to meticulously trace anatomical structures slice by slice. This manual intervention has several critical drawbacks. It is time-consuming as it can take hours per patient, and subjective as the result depends on the individual operator. Also, this step hinders the potential for data-driven discovery and the development of more personalized medical interventions.

This project aims to overcome these limitations by validating an automated pipeline for the quantitative analysis of bone morphology from CT scans. By leveraging Machine Learning and advanced image processing techniques in Python, the goal is to conduct a statistical analysis of cortical bone thickness development in the tibiae of children, using data extracted from measurements made by the algorithm.

The specific application scope of this thesis is the analysis of measured cortical tissue thickness in pediatric tibiae, using a dataset provided by the Children's

Hospital of Philadelphia (CHOP). The project will build upon the foundational code by Alberto Sánchez Bonastre, a former ICAI student [1].

1.1 Project motivation

The intersection of medical imaging and computational analysis is currently driving a paradigm shift in healthcare, moving towards more quantitative, personalized, and preventative medicine. The main motivation for this project is to contribute to this evolution by addressing the challenges and opportunities presented by the analysis of Computed Tomography (CT) scans, particularly in the specialized field of pediatric bone development.

The Clinical Need and Current Limitations

At present, the analysis of CT image analysis for metrics such as bone cortical thickness relies heavily on manual or semi-automated processes. While essential for diagnosis and research, these methods are inherently problematic. They are not only time-consuming and labor-intensive, requiring hours of intervention by highly trained radiologists, but are also susceptible to significant inter-observer and intra-observer variability. This lack of consistency and efficiency creates a bottleneck that limits the scale of clinical studies and hinders the routine application of quantitative analysis in patient care. This project proposes a fully automated framework to overcome these limitations, aiming to validate and analyze the measurements made of cortical thickness, both rapid and highly reproducible.

Contribution to Research and Innovation

From a research perspective, this work is motivated by the need for robust and generalizable tools that require minimal human intervention. By validating an automated algorithm for segmentation and measurement, this project contributes directly to the advancement of medical image processing. This aligns with the broader goals of technological progress, as outlined in the UN's Sustainable Development Goal 9 (Industry, Innovation, and Infrastructure), by creating an innovative and effective solution to a persistent challenge in medical diagnostics. The automation of this process will enable large-scale demographic studies of bone development in children, allowing for novel investigations into correlations with age, gender, and other environmental or physical factors.

Furthermore, this study Establishing these normative growth patterns is crucial for the early detection of skeletal diseases and for monitoring the effects of therapeutic interventions.

Societal and Clinical Impact

Beyond the technical innovation, there is a strong ethical motivation to contribute to medical and social progress. This project contributes valuable data to the understanding of cortical bone thickness development in children, a relatively under-researched field. Furthermore, it is directly aligned with several key societal goals (the UN's Sustainable Development Goals that is aligned with are also explained in Annex I):

- **Good Health and Well-being (SDG 3):** By providing a tool for precise and effortless measurement of cortical thickness, this work has numerous beneficial medical applications. It can enhance the monitoring of pediatric conditions like osteosarcoma or osteogenesis imperfecta, track treatment efficacy for therapies involving calcium supplementation, and provide deeper insights into the fundamental processes of bone development during childhood.
- **Reduced Inequalities (SDG 10):** Automating diagnostic processes can significantly reduce the costs associated with clinical judgment by minimizing the hours required for manual analysis. This, in turn, can make advanced diagnostic technology less expensive and more accessible to a wider population, regardless of geographic location or economic status.

Potential Applications

Ultimately, the development of a robust automated system for measuring cortical thickness serves as a foundation for numerous future applications. The primary incentives for this work include:

- **Clinical Disease Monitoring:** Tracking the progression of bone diseases and the patient's response to treatment over time with high precision.
- **Pharmacological Research:** Quantitatively assessing the effects of medications designed to improve bone density or calcium deposition.
- **Large-Scale Epidemiological Studies:** Creating vast datasets to detect patterns and correlations between bone thickness and various demographic, genetic, or environmental variables.
- **Surgical Planning:** Generating accurate 3D models of bones to aid in the preparation for complex traumatological or orthopedic surgeries.
- **Foundation for Predictive AI:** The quantitative data produced by this tool can be used to train supervised machine learning algorithms focused on predicting future fracture risk or identifying biomarkers for latent diseases.

Chapter 2

Description of the technologies

It is necessary to have some previous knowledge of the technological background in the field of medicine and computerization to keep track of the process that has been performed.

2.1 Computed Tomography (CT)

Computed Tomography, commonly known as a CT scan, is an advanced medical imaging technique that provides detailed, non-invasive views inside the human body.

2.1.1 Fundamental Principles

Invented in the 1970s by Sir Godfrey Hounsfield, CT imaging fundamentally improves upon traditional X-rays. While a conventional X-ray produces a single 2D projection (a shadowgram where anatomical structures are superimposed), a CT scanner acquires multiple projections from different angles. This is achieved by a rotating gantry, which houses an X-ray source on one side and an array of sensitive detectors on the opposite side. As the gantry rotates around the patient, it captures hundreds of X-ray attenuation profiles.

The "computed" aspect of the name refers to the crucial next step: a powerful computer uses sophisticated mathematical algorithms, most commonly filtered back-projection, to reconstruct these multiple 2D projections into a detailed 3D volumetric dataset. This volume is composed of a stack of 2D cross-sectional images, or *slices*. These slices can then be visualized and analyzed in any plane—typically axial, sagittal, and coronal—allowing for a comprehensive anatomical assessment without the issue of overlapping structures. For this project, the 3D nature and

high resolution of CT are indispensable for the precise morphological analysis of bone.

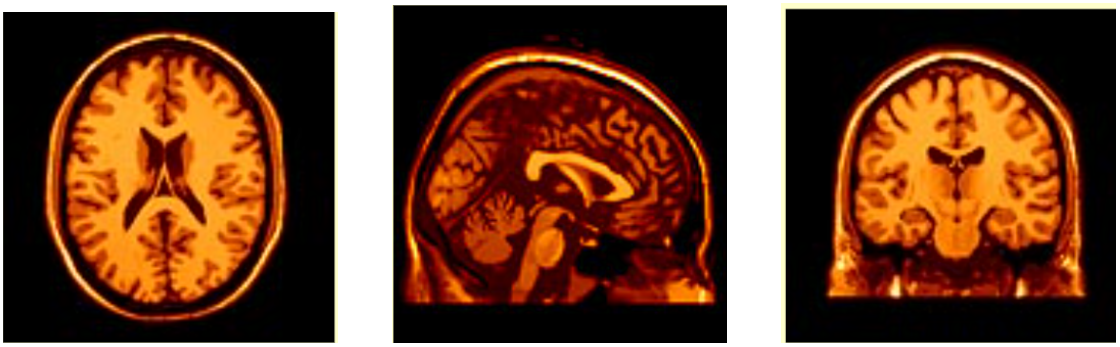

(a) Axial Plane (b) Sagittal Plane (c) Coronal Plane

Figure 2.1: The three standard anatomical planes used in medical imaging. Images adapted from Chudler [2].

2.1.2 DICOM

Digital Imaging and Communications in Medicine (DICOM) was developed by the American College of Radiology (ACR) and the National Electrical Manufacturers Association (NEMA) in 1980. Now, it has become an international standard for storing medical imaging information, as well as protocols for sharing its data.

DICOM is made of both the images and the metadata (information from the image and the patient, such as age, gender, etc.). It is used to share this information between different devices, like scanners and hospital servers.

The main advantage of DICOM is how safe it is compared to other systems. As medical information is sensitive, it must have strict protocols to meet the requirements of data protection.

2.1.3 Hounsfield Units

The Hounsfield Units (HU) are a scale used in CT imaging to measure radiodensity. This is, HU quantifies how much X-rays can be absorbed or blocked by the structure. This helps differentiate between different types of body tissues. Thus, they are strongly relevant in this project in the reconstruction of 3D bones. For instance, air is -1000 HU, and water is 0 HU. Dense bone can be ≥ 1000 HU.

With these units, the bone tissue can be filtered and selected from the other parts of the leg.

Tissue	Hounsfield Units (HU)	Description
Air	-1000	Very low density
Fat	-100 to -50	Low density
Water	0	Reference point
Muscle	+30 to +70	Soft tissue
Bone	+700 (cancellous bone) to +3000 (cortical bone)	Very dense

Table 2.1: Typical Hounsfield Unit values for various tissues [3].

2.2 Image Processing

Digital image processing is analyzing the types of files and its data related to images with different techniques.

2.2.1 Morphological Operators

The morphological operators are image processing techniques used primarily in binary and grayscale images to analyze and manipulate the structure or shape of objects within an image. They are widely used in fields like medical imaging, computer vision, and pattern recognition.

Morphological operations use a structuring element that slides over the image to probe and modify pixel values based on the shape and size of the element.

The two inputs of the operators are the original image and a *kernel*. A *kernel* (also called a filter or convolution matrix) is a small matrix used to apply effects like blurring, sharpening, edge detection, and more to an image.

The core morphological operations are erosion, dilatation, opening, closing, morphological gradient, and top-hat and black-hat transformations.

Among the various applications of these morphological operators for creating masks for the project, boundary extraction and region filling are particularly noteworthy.

Erosion

In erosion, the kernel (matrix) moves across the image. For each position, it checks whether all pixels under the kernel (where the kernel has a value of 1) match the foreground. If all match, the central pixel remains foreground. If any pixel under the kernel is background (black or value 0), the central pixel is set to background.

Erosion shrinks bright regions and removes small white noises. In medical imaging, it is used to clean bone structures (as we did).

Dilatation

Conversely, dilatation is used to expand or grow the boundaries of foreground regions in a binary or grayscale image. When a kernel slides over the image, if any pixel under the kernel is foreground, the center pixel becomes foreground.

This causes objects to grow outward, filling small holes and connecting nearby objects.

$$\begin{bmatrix} 1 & 1 & 1 \\ 1 & 1 & 1 \\ 1 & 1 & 1 \end{bmatrix}$$

Figure 2.2: Commonly used kernel in morphological operations such as erosion and dilation.

The segmentation process begins with an initial erosion operation to remove small impurities and noise from the image. This is followed by a dilation step to restore the original bone structures. A second erosion is then applied to eliminate any residual artifacts introduced during the previous dilation. Finally, a concluding dilation is performed to generate the binary masks. The result after applying a predefined threshold is the final segmented bone structure.

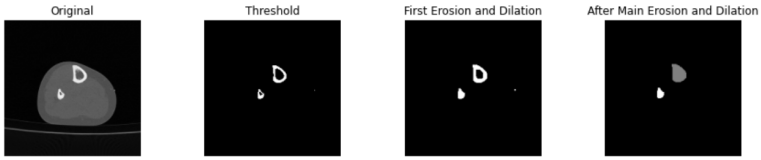

Figure 2.3: Visual example of erosion and dilation morphological operators.

2.2.2 Gaussian filters

A Gaussian filter is a low-pass filter used to reduce noise and blur images. It operates by smoothing the image, effectively eliminating pixels with anomalous intensity levels compared to their neighbors—noise which may originate during image acquisition or transmission. Its operation is based on the principle of convolution, where each pixel's value is replaced by a weighted average of the pixels surrounding it.

Unlike a simple mean filter, where all neighboring pixels contribute equally, a Gaussian filter assigns weights based on a Gaussian function (a "bell curve"). This

ensures that pixels closer to the center of the kernel have a significantly higher influence on the output value than pixels farther away. This behavior mimics how real-world signals often attenuate, making it a very natural way to smooth data.

In practice, the filter is implemented as a *kernel*, which is a small matrix of numbers derived from the Gaussian function. The kernel is centered on a pixel, and the values of the surrounding pixels are multiplied by the corresponding kernel values. These products are then summed up to get the new value for the central pixel. This process, known as convolution, is repeated for every pixel in the image.

For example, a simple 3x3 Gaussian kernel might look like this:

$$\frac{1}{16}\begin{bmatrix}1 & 2 & 1\\ 2 & 4 & 2\\ 1 & 2 & 1\end{bmatrix}$$

Notice how the central value (4) is the highest, and the values decrease as you move away from the center.

The primary effects and applications of applying a Gaussian filter are:

- **Noise Reduction:** The filter is highly effective at reducing random noise (like Gaussian noise) in an image, as it averages out anomalous pixel values.

- **Image Smoothing:** It creates a smooth, "blurry" effect by reducing sharp transitions and fine details. This is often a necessary pre-processing step for other computer vision tasks.

- **Edge Detection:** Because it suppresses fine details, a Gaussian filter is often applied before edge detection algorithms (like the Canny edge detector) to prevent the algorithm from detecting false edges caused by noise.

In short, a Gaussian filter is a fundamental technique for cleaning up images by applying a "smart" blur that prioritizes nearby pixels.

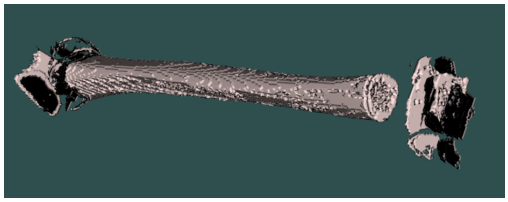

(a) Original Image with Noise

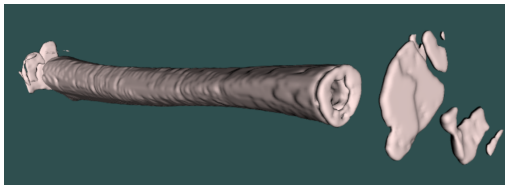

(b) Image After Gaussian Filter

Figure 2.4: Visual effect of applying a Gaussian filter to an image for noise reduction.

2.3 STL files

STL ("*Stereolithography*") is a 3D file format widely used for modeling and printing. It describes the surface geometry of a 3D object using a mesh of triangles. These triangles are defined by three vertices and a normal vector. The complex the figure, the more triangles will need to be used. However, STL files do not contain color, texture, or material information.

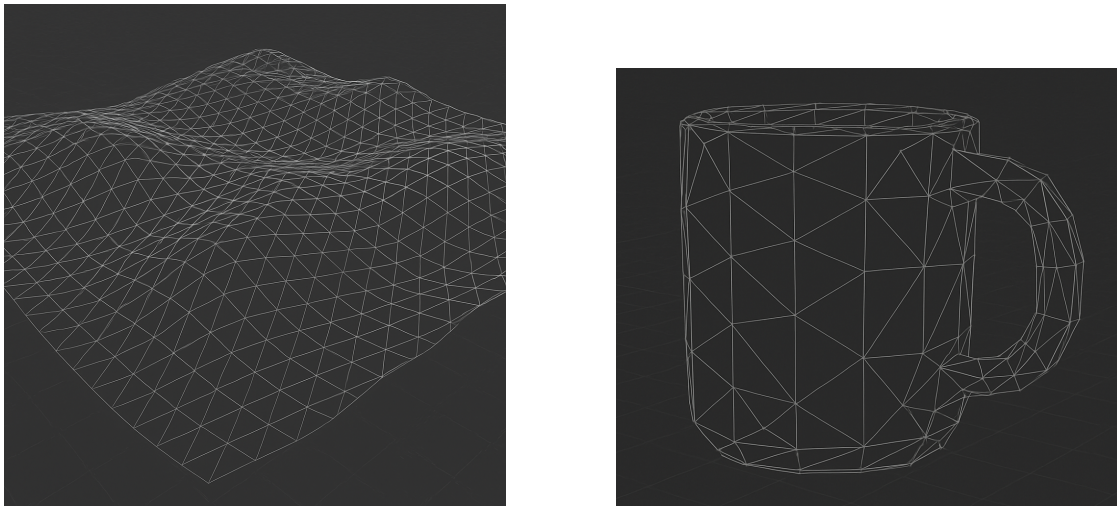

Figure 2.5: STL mesh

STL files are commonly used for 3D printing, CAD software, and simulation and analysis.

2.4 Segmentation

Image segmentation is the process of partitioning an image into distinct and meaningful regions that correspond to different anatomical structures or areas of interest. It plays a fundamental role in medical imaging, serving as a critical preprocessing step for almost all post-processing tasks, including measurement, visualization, and diagnosis.

Traditionally, segmentation masks were created manually by clinicians or technicians to isolate the target anatomical regions from the full image. This manual process is not only time-consuming but also prone to variability, depending on the operator's expertise and the characteristics of each individual case.

Classic segmentation methods rely on morphological operators and conventional image processing techniques. While effective in many cases, these methods typically require manual adjustment of parameters, such as thresholds and kernel sizes, which may differ significantly from one patient to another.

To reduce human intervention and improve generalization, heuristic approaches such as *K-Means* clustering have been introduced. While *K-Means* offers a straightforward and computationally efficient solution for unsupervised pixel classification, it lacks robustness and generalization when applied across diverse datasets, limiting its utility in more complex or variable clinical scenarios.

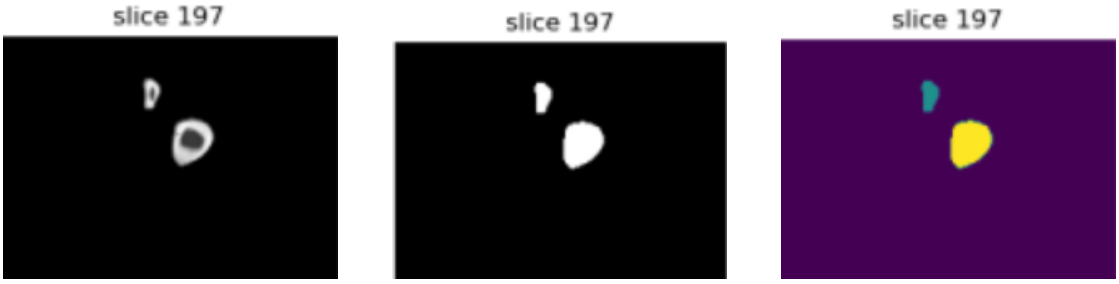

(a) Original (b) Segmented (c) Masks

Figure 2.6: Process of segmentation and masks labeling

2.4.1 Deep Learning masks

Artificial Intelligence (AI) strategies offer an automatic way that saves time performing this task through segmentation. Deep Learning can obtain morphologic

segmentation from medical images.
This process is more generalizable, as it is a training process.
An example of Deep Learning masks can be found in this article [4]. With a combination of MRI scans, gliomas (brain tumors) can be accurately segmented, along with an estimation of the patients' overall survival rate. It employs 2D volumetric convolution neural network architectures that utilize a majority rule. The results obtained are quite satisfactory and promising.

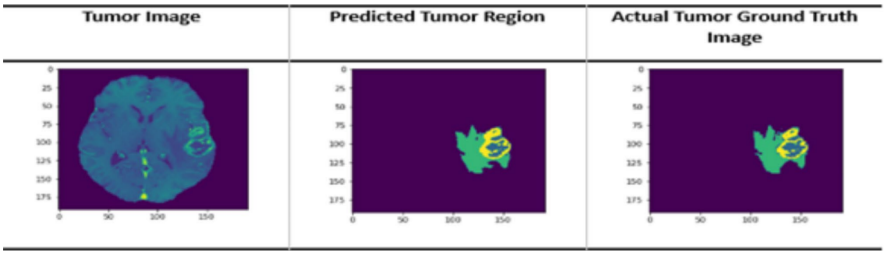

Figure 2.7: Example of automated brain tumor segmentation using a deep learning model. The model generates a colored mask to identify different tumor regions (enhancing tumor, necrotic core, and edema). Image adapted from [4].

2.5 Hausdorff Distance

The Hausdorff distance is a metric used to measure how far two non-empty subsets of a metric space are from each other. In the field of medical image segmentation, it has become a standard tool for comparing a segmented result (e.g., a predicted mask) with a ground truth annotation. It measures the maximum distance from a point in one set to its closest point in the other set.

Informally, two sets are close in the Hausdorff distance if every point in either set is near some point in the other set. It can be thought of as the longest distance an adversary would be forced to travel when choosing a point in one set and moving to the closest point in the other.

Interpretation in Medical Segmentation

In the context of evaluating segmentation accuracy, the Hausdorff distance is a measure of boundary disagreement.

- **A low value** indicates that the boundaries of the predicted segmentation and the ground truth are very close everywhere. A value of 0 would mean the sets of points are identical.

- **A high value** indicates a significant discrepancy at one or more points along the boundary.

A key property of the Hausdorff distance is its high sensitivity to outliers. A single, erroneously segmented pixel far away from the true boundary can result in a very large Hausdorff distance, even if the rest of the segmentation is perfect. While this can be a drawback, it also makes it an excellent metric for applications where every point must be accurately captured, such as in clinical settings for surgical planning or radiation therapy.

2.6 Smoothing

The smoothing process is applied to improve the quality of the generated 3D mesh by enhancing the shape of individual cells and promoting a more uniform distribution of vertices. This results in a cleaner, more visually consistent surface, which is particularly beneficial for subsequent analysis or visualization.

To achieve this effect, the `vtkWindowedSincPolyDataFilter` class from the `VTK` library is used. This filter performs smoothing through interpolation, adjusting the position of each point in the mesh based on its neighbors while preserving the overall geometry. The windowed sinc function offers control over the degree of smoothing and maintains important anatomical features by minimizing surface shrinkage.

2.7 SDF (Signed Distance Function)

A Signed Distance Function (or Signed Distance Field) is a powerful method for representing a shape implicitly in space. Unlike an explicit mesh representation like an STL file, which only describes the surface, an SDF provides volumetric information about the entire space surrounding the object.

For any given point in space, an SDF returns the shortest Euclidean distance from that point to the surface of a shape. The "signed" aspect is the most crucial property:

- **Positive Value:** The point is outside the shape.
- **Negative Value:** The point is inside the shape.
- **Zero Value:** The point lies exactly on the shape's surface.

This provides a rich, continuous field of information. The surface of the shape itself is known as the zero-level set of the function. A key advantage of this representation

is that certain geometric operations become very efficient. For instance, the normal vector at any point on the surface can be calculated by finding the gradient of the SDF, $\nabla f(x)$.

Applications in Medical Image Processing

SDFs are particularly useful in medical imaging and computational geometry for several reasons:

- **Robust Shape Representation:** They can be generated directly from binary segmentation masks and can represent complex topologies without the connectivity constraints of a mesh.

- **Geometric Measurements:** An SDF allows for robust calculation of geometric properties. In the context of this project, it could be used to analyze the thickness and curvature of the cortical bone in a continuous manner.

- **Mesh Generation and Smoothing:** High-quality, smooth 3D meshes can be generated from an SDF by using algorithms like Marching Cubes on the zero-level set.

- **Image Registration:** SDFs can be used to align or register different shapes by minimizing the distance between them.

From the original segmented image, both the inner and outer contours of the bone are computed. The region between these two contours represents the cortical bone, often referred to as the "skeleton" in this context.

To quantify cortical thickness, a Signed Distance Function (SDF) is computed relative to the inner contour. This function estimates the shortest distance from each point on the inner surface to the corresponding point on the outer surface. The maximum of these distances corresponds to the Hausdorff distance, which serves as a robust geometric descriptor of cortical thickness across the structure.

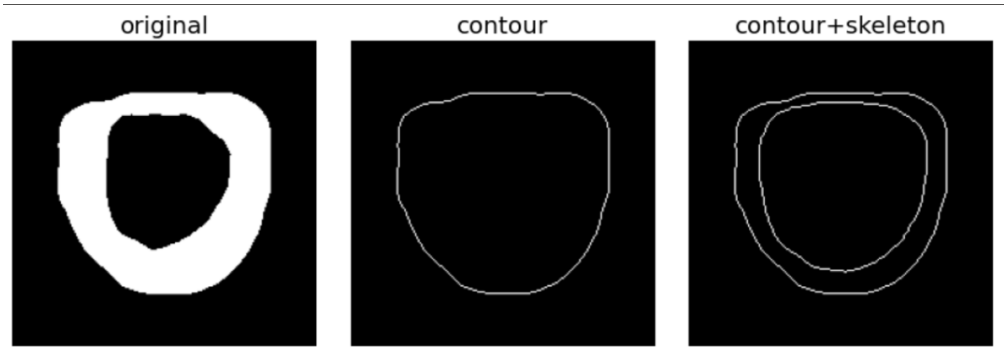

Figure 2.8: Original binary mask of the shape.

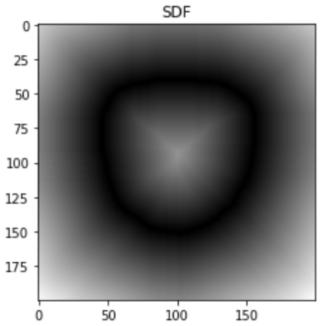

Figure 2.9: Resulting Signed Distance Field (SDF).

Both figures from [5]

2.8 3D Slicer

3D Slicer is a free, open-source software platform for analyzing, visualizing, and editing medical images, such as MRI and CT scans. It features functions such as image segmentation and DICOM support for clinical imaging data, which we have utilized in our project.

2.9 Jupyter, Python

Jupyter is an open-source tool that enables to create and share notebooks, which can contain code, text, equations, visualizations, etc. It uses Python as one of the coding languages. In our project, different libraries had to be implemented, such as NumPy (Numerical Python), used for numerical computing, or OpenCV (Open Source Computer Vision), for real-time computer vision and image processing.

2.10 Agile

Agile is a work methodology that allows for quick responses to reviews. It has its foundation in four bullet points:

- People and interactions are the priority.
- Perfect operation of the product.
- Collaborate with the client.
- The work process must always respond to change.

Scrum is a specific way to implement Agile. It provides a structured process to deliver work in small *sprints*. In addition, a backlog is a prioritized list of work that needs to be done.

Chapter 3

State Of Art

The first study of computed tomography (CT) scans was carried out by Godfrey N. Hounsfield at the EMI Central Research Laboratories in London, England. While conducting his research, Godfrey deduced that X-ray measurements of a body taken from different directions would allow for the reconstruction of its internal structure. According to Hounsfield's estimates, an accuracy of 0.5% could be achieved in the X-ray attenuation coefficients for each slice. [6]

In 1971 arrived at the clinical field the computed tomography as an X-ray technique that could only produce axial images of the brain, which was relevant for neuroradiology. Over time, scanners were developed that could be applied to other parts of the body. The first to appear were axial scanners with a single row of detectors in 1976. Later, the technology advanced to helical or spiral scanners, allowing the use of equipment with multiple rows of detectors, which are now commonly used in clinical practice.

This scanner method has been improving in terms of space, time, and ability. It has also been evolving from a traditional anatomic modality to a functional one. This means, a modality of detection and measurement of changes in the metabolism, blood flow, or chemical composition.

Now the CT is a versatile technique, able to create 3D images of different anatomic fields like oncology, cardiology or traumatology among others. For both the diagnosis and the patient follow-up analysis, radiotherapy treatment, and even for screening asymptomatic subpopulations with specific risk factors.

In 2017, Howard Chen published the article "DICOM Processing and Segmentation in Python", in which he used Hounsfield units (HU) to reconstruct and analyze lungs. Starting from raw DICOM files obtained from a patient, he extracted voxel data into NumPy arrays and generated a histogram to analyze the content of the DICOM images and remove unwanted elements, such as air, leaving the lungs. [3]

Chen resampled the images to ensure that each slice had a uniform resolution of 1x1x1 mm in pixels and planes. Using various functions, he identified the

appropriate threshold by creating two KMeans clusters that differentiated between soft tissue/bone and lung/air. With erosion and dilation techniques, he removed small features such as pulmonary vessels and noise, and labeled each distinct region as a separate image. Then, he used bounding boxes for each image label to identify which ones corresponded to the lungs and which did not, creating masks to isolate the pulmonary areas. He applied this mask to the original image to remove voxels outside the lung fields and, with all this information, generated a three-dimensional representation of the DICOM image.

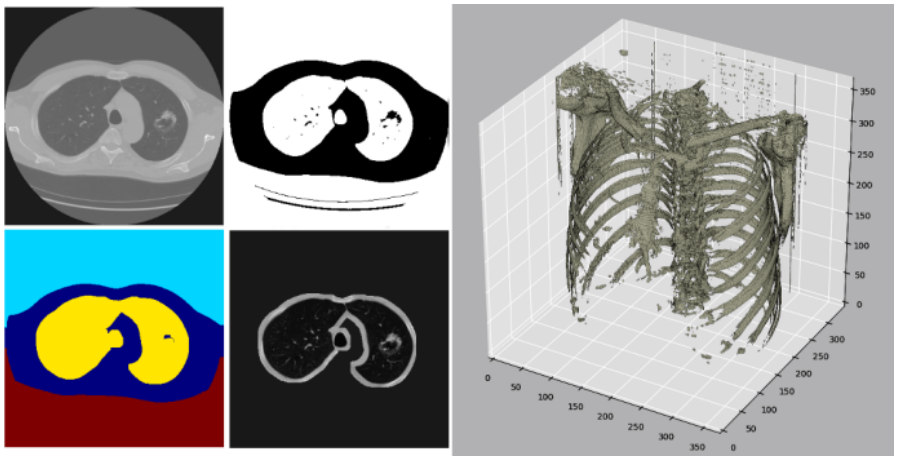

Figure 3.1: CT segmentation and 3D reconstruction steps. Image adapted from Howard Chen's blog post *DICOM Processing and Segmentation in Python* [3].

In 2018, Wenjing Du, Jinhuan Zhang, and Jingwen Hu presented an innovative local thresholding method in their article "A Method to Determine Cortical Bone Thickness of Human Femur and Tibia Using Clinical CT Scans" to measure cortical bone thickness using clinical CT scans. This approach uses statistical models that take into account cortical bone thickness in the femur and tibia based on variables such as sex, age, height, and body mass index (BMI). The study emerged because of the often-failed global thresholding method to provide accurate estimates of cortical bone thickness in areas where the cortex is thinner. The new local thresholding method showed an average thickness estimation error of less than 0.1 mm and demonstrated greater accuracy in thin cortex areas compared to the global thresholding method. Statistical analysis results revealed that both age and BMI significantly influence cortical bone thickness in the femur and tibia. In the global thresholding method, a fixed HU value is applied to all value-location profiles, considering values above the threshold as cortical bone and those below as non-cortical bone. [7]

A year later, in 2019, Wojtek Rosa presented in "Advanced DICOM-CT 3D Visualizations with VTK" a method for creating three-dimensional visualizations

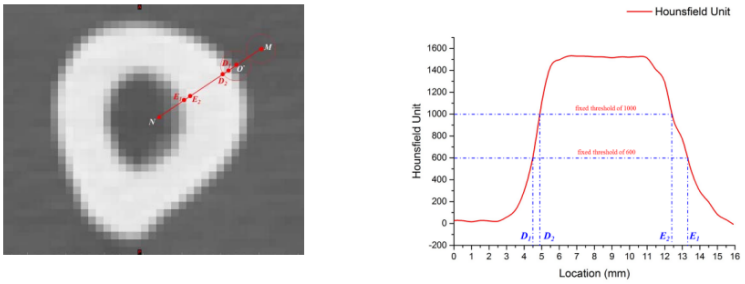

Fig. 3. Cortical bone thickness estimation based on the global thresholding method.

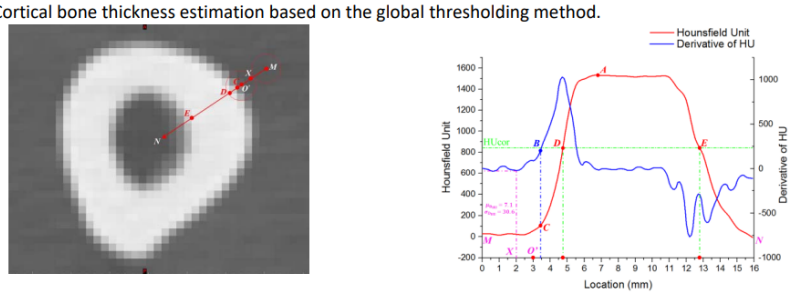

Fig. 4. Cortical bone thickness estimation based on the local thresholding method.

Figure 3.2: Local and global thresholding method from [7] project.

of DICOM data obtained through CT, using the VTK library to represent the lungs, skeleton, and circulatory system. Limitations arose related to data size, interactivity and performance, data compatibility, and system performance when working with interactive 3D visualizations. [8]

Shingo Ota and his team published the article "Cortical thickness mapping at segmented regions in the distal radius using HR-pQCT" where they developed a method for cortical thickness apping using high-resolution peripherial quantitative computed tomography (HR-pQCT). Their approach segmented the distal radius (forearm near the wrist) into dorsal, palmar, radial, and ulnar regions, enabling localized analysis of cortical thinning. The study revealed significant age-related changes in cortical thickness and porosity, particularly in the dorsal and palmar regions, offering a sensitive tool for detecting early signs of osteoporosis. [9]

In 2023, Alberto Sánchez - Bonaste, in the article "Systematic Measuring Cortical Thickness in Tibiae for Biomechanical Analysis" [1], developed an algorithm capable of reading CT images and measuring cortical bone thickness. To achieve this, they used classical morphological segmentation, interpolation to clean the bone structure, and signed distance functions (SDF) for measuring cortical thickness. As a result, comparing it with measurements taken by a radiologist, the differences had a mean of 0.25 mm and a standard deviation of 0.2.

Also in 2023, a study introduced an analysis-by-synthesis method for modeling cortical bone from clinical QCT scans. This technique addresses limitations in

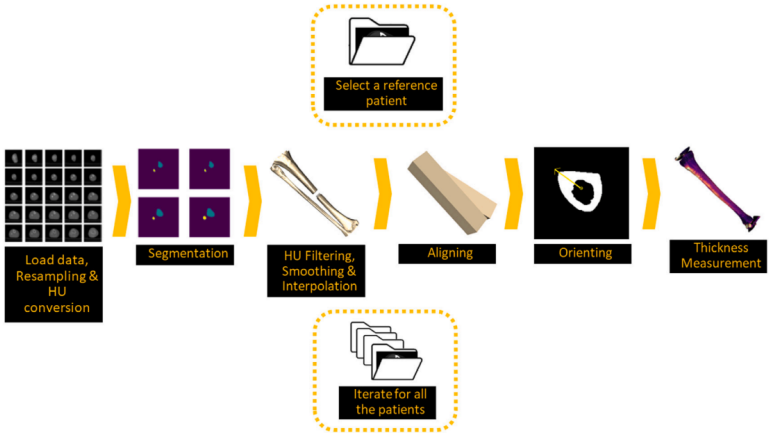

Figure 3.3: Diagram of the process from [1].

spatial resolution and partial volume effects by simulating the imaging process and fitting a model to observed data. The result is a more accurate estimation of cortical thickness, especially in vertebral bones, enhancing the reliability of clinical assessments and biomechanical modeling. [10]

In 2024, Valentina Campanelli and Maury L. Hull published an article titled "Unbiased Method to Determine Articular Cartilage Thickness Using a Three-Dimensional Model Derived from Laser Scanning: Demonstration on the Distal Femur", in which they presented a technique capable of recreating a 3D model of articular cartilage. Their goal was to measure cartilage thickness on the articular surfaces of long bones such as the femur. To do this, they incorporated the articulated cartilage into CT scans to enable the study of knee kinematics. The method involved laser scanning, and with the use of fiducial markers, they measured cartilage thickness, which ranged between 1.5 mm and 2.0 mm. The results showed negligible bias and a precision of 0.13 mm. Prior to this study, achieving highly accurate results with existing methods required the removal of cartilage. The described technique is invasive and relies on lasers as the scanning method to explore the surface of the distal femoral joint, with a resolution range between 67 and 92 microns. This method can introduce systematic errors or significant biases due to dimensional issues of the underlying bone. [11]

This new technique offers greater precision in measurements compared to threshold-based methods, which are unreliable for detecting the cortex in the sub-millimeter range - something clinically relevant.

Chapter 4

Work Definition

4.1 Reasoning

In recent years, numerous algorithms and software tools have been developed to support the medical field by accelerating workflows and improving both efficiency and accuracy. Despite these advancements, medical image analysis is still often performed manually by experts—a process that can take anywhere from several hours to multiple days and is inherently prone to human error.

Alberto Sánchez Bonastre and his team [1] developed an algorithm with the aim of automating morphological segmentation in medical images. While their work laid the foundation for automation, it was limited by the lack of a sufficiently large and diverse dataset. As a result, they were unable to identify meaningful patterns or correlations between bone morphology and patient-specific variables such as age, height, weight, or broader demographic factors, including ethnicity and diet.

Moreover, the development of long bones in children remains an area that requires further investigation. Understanding how cortical bone thickness evolves during growth could have important diagnostic and therapeutic implications.

The present project builds upon this initial work, aiming to fully automate the segmentation and measurement processes to improve accuracy, generalization, and scalability. By refining the segmentation algorithms and enhancing the measurement pipeline, the objective is to create a more robust and clinically useful tool.

With this algorithm, a statistical analysis is made to contribute to the knowledge of the cortical tissue thickness development in children's tibiae. It could have numerous medical applications, for instance, it could be used to monitor cortical bone changes in pediatric patients with osteosarcoma or other bone-related conditions, providing a means to evaluate disease progression or treatment efficacy. It may also serve to study early-stage bone development or assess the effects of calcium supplementation on cortical tissue quality. Furthermore, when combined

with longitudinal patient data, cortical thickness could potentially act as a proxy biomarker for the early detection of skeletal or metabolic disorders.

4.2 Goals

Project Objectives

General Objective

To make the statistical analysis of bone thickness development in children's tibiae with two different methods, validating an automated image analysis algorithm capable of segmenting anatomical structures and measuring cortical bone thickness from CT scans, with applications in pediatric orthopedic imaging.

Primary Objectives

1. To improve a fully automated algorithm for the segmentation of the tibia and the measurement of its cortical thickness from clinical CT scans.

2. To apply the algorithm to a pediatric CT image database in order to perform a demographic study of cortical bone development, examining correlations with variables such as age and gender.

3. To make a comparison of the different measurement methods used and check which one is more reliable.

By achieving these goals, this work will provide a valuable tool for both clinical research and potential future diagnostic applications in pediatric orthopedics.

4.3 Methodology

For the development of this project, an Agile methodology will be adopted through the implementation of a simplified version of Scrum. In this setup, daily meetings will be omitted in favor of biweekly sessions to define the goals for each new *sprint*. Sprint and backlog management will be carried out using the Planner tool integrated in Microsoft Teams.

The primary aim is to refine and validate an algorithm capable of automatically segmenting DICOM medical images and accurately measuring cortical bone thickness. The algorithm will be enhanced in terms of segmentation efficiency,

measurement accuracy, and the quality of labeling and anatomical localization. The final solution is intended to support both orthopedic and dental applications.

The development will follow an iterative structure broken into key phases:

1. **Preliminary Research and Familiarization:** A thorough review of the existing literature and related works will be conducted. In this phase, previous contributions—particularly the algorithm developed by Alberto Sánchez will be analyzed. The researcher will also gain proficiency in Python, GitHub, and the associated libraries and code base. (*6 weeks*)

2. **Data Preprocessing:** The CT image datasets provided by the Children's Hospital of Philadelphia will be examined and exported. Invalid images will be discarded, and any necessary preprocessing (cropping, normalization, metadata correction) will be applied. (*16 weeks*)

3. **Analysis of Social and Demographic factors:** Deep research will be carried out to decide the age ranges and other factors connected to bone thickness. (*3 weeks*)

4. **Segmentation Pipeline Development:** The existing segmentation code will be tried and improved to address current limitations. Classical morphological segmentation will be optimized and tested with the database collected. (*6 weeks*)

5. **Evaluation:** Conclusions and comparisons between methods and thicknesses will be made. (*4 weeks*)

6. **Thesis Writing:** Documentation and drafting of the final thesis will occur in parallel with the technical work, but intensive writing will continue throughout and after implementation. (*38 weeks*)

The entire process will be carried out using a combination of tools and technologies:

- **Python (via Anaconda)**: For some algorithm corrections, using libraries such as `NumPy`, `OpenCV`, `Pandas`, `VTK`, and `Pydicom`.
- **3D Slicer**: For advanced medical image visualization and comparison of segmentation results.
- **GitHub**: For version control and collaboration.
- **Microsoft Teams + Planner**: For communication, task planning, and sprint tracking.

- **Hardware**: A Lenovo IdeaPad Gaming 3 laptop with sufficient computational resources for training and testing.

The schedule followed was this one:

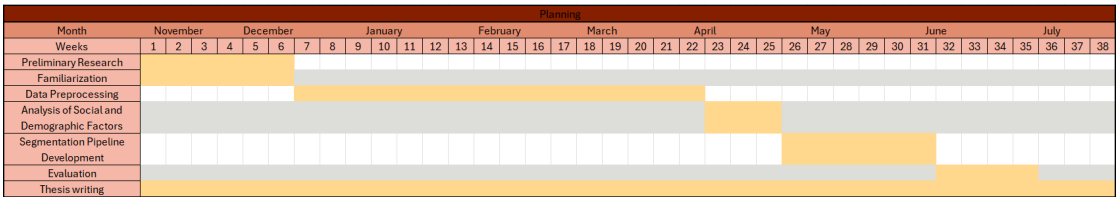

Figure 4.1: Planning and Workflow Diagram

4.4 Economic Study

Even though the project had zero costs, the value of the laptop used decreased due to usage and time.

- Asset: Lenovo IdeaPad Gaming 3 Laptop
- Fiscal Useful Life: According to the amortization tables of the Spanish Tax Agency, computer equipment has a useful life of 4 years (208 weeks).
- Purchase Value: 1000 €
- Duration of the Project: 38 weeks

Amortization cost per week:

$$1,000.00€/208\text{weeks} = 4.81€$$

For the 38 weeks the equipment depreciation cost is:

$$4.81€ * 38\text{weeks} = 182,78€$$

Added to this, the personnel costs.. According to the ECTS credit system and following the regulations of the Comillas Pontifical University (ICAI), the time dedication is calculated as follows:

- Project Credits: 6 ECTS
- Hours per credit: 25 hours

Total hours calculation:

$$6\text{ECTS} * 25 \text{ hours/ECTS} = 150\text{hours}$$

The gross annual salary estimated of a recently graduated engineer is 27,000 € with 1,800 annual work hours:

$$27,000€/1,800 \text{ hours} = 15.00€/\text{hour}$$

Plus Social Security Costs (30% employer contribution):

$$15.00€ * 1.30 = 19.50€/\text{hour}$$

The total personnel cost is:

$$150\text{hours} * 19.50€/\text{hour} = 2,925.00€$$

To sum up, the total project cost is the sum of the depreciation and personnel costs:

$$182,78.00€ + 2,925.00€ = \textbf{3,107.78 €}$$

Chapter 5

Developed Model

5.1 System Analysis

The project has been carried out in tibia bones, although same techniques described in the document could probably be applied to other long bones such as femur and ulna.

The processing pipeline consists of two main stages. In the first stage, the DICOM files are analyzed to reconstruct a three-dimensional representation of the bone. This 3D model is then exported as an STL file, which serves as a standardized geometric format for further processing.

In the second stage, the generated STL file is loaded, aligned, and oriented with respect to a predefined reference bone. Once aligned, the bone is segmented into multiple cross-sectional profiles, and cortical thickness is measured across these sections. The results are saved in two output formats: Pickled files, which store individual profile data, and NumPy arrays, which represent thickness measurements in matrix form.

After this measurement step, a correction procedure is applied to account for any bones that were misaligned or originate from the contralateral leg (i.e., the opposite side), ensuring that all samples are standardized relative to the reference orientation. For the statistical analysis, scatterplots and Bland-Altman plots have been generated to compare the two methods studied and check whether the study is biased or not. Additionally, an analysis is conducted comparing gender and age ranges.

5.2 Sample

The database was provided by the Children's Hospital of Philadelphia (CHOP) through SQL tables. To acquire the patients and their information, two queries

were generated.

5.2.1 Explanation of the Query

The query follows a step-by-step execution flow, where each Common Table Expression (CTE) (WITH statements) processes and aggregates data before joining everything to the patient table. The first part of the query collects patient's data such as medications, gender, ethnicity, country, state, marital status, religion and whether it has been seen in the last two years or not.

Listing 5.1: SQL Query database and medications

```
-- Step 1: Aggregate Medications First
WITH Medications AS (
    SELECT
        mo.pat_id,
        STRING_AGG(DISTINCT m.med_name, ', ') AS medications
           ,
        STRING_AGG(DISTINCT m.form, ', ') AS
           medication_forms,
        STRING_AGG(DISTINCT m.pharm_class_code, ', ') AS
           pharm_class_codes,
        STRING_AGG(DISTINCT m.pharm_subclass_code, ', ') AS
           pharm_subclass_codes
    FROM arcus.medication_order mo
    JOIN arcus.medication m ON mo.med_id = m.med_id
    GROUP BY mo.pat_id
)

-- Step 2: Join Everything Efficiently
SELECT
    p.pat_id,
    p.sex_abbr,
    p.ethnicity,
    p.country,
    p.state,
    p.seen_last_two_yrs_ind,
    p.marital_status,
    p.religion,
    COALESCE(m.medications, 'None') AS medications,
    COALESCE(m.medication_forms, 'None') AS medication_forms
       ,
    COALESCE(m.pharm_class_codes, 'None') AS
       pharm_class_codes,
```

```
    COALESCE(m.pharm_subclass_codes, 'None') AS
       pharm_subclass_codes,

FROM arcus.patient p
LEFT JOIN Medications m ON p.pat_id = m.pat_id;
```

1. Step 1: Aggregate medications (Medications CTE)

Listing 5.2: Step 1: Aggregate medications

```
WITH Medications AS (
    SELECT
        mo.pat_id,
        STRING_AGG(DISTINCT m.med_name, ', ') AS
           medications,
        STRING_AGG(DISTINCT m.form, ', ') AS
           medication_forms,
        STRING_AGG(DISTINCT m.pharm_class_code, ', ') AS
            pharm_class_codes,
        STRING_AGG(DISTINCT m.pharm_subclass_code, ', ')
            AS pharm_subclass_codes
    FROM arcus.medication_order mo
    JOIN arcus.medication m ON mo.med_id = m.med_id
    GROUP BY mo.pat_id
)
```

(a) medication_order (mo):

- Extracts mat_id (linking to patient table).
- Extract med_id (links to medication table).

(b) JOIN medication (m) ON mo.med_id = m.med_id:

- Retrieves medication details for each med_id

(c) GROUP BY mo.pat_id:

- Aggregates all medications per pat_id.
- Uses STRING_AGG() to store multiple medication names, forms, and classes in comma-separated lists.

Field name	Description	Source Table
Pat_id	Patient ID	Medication_order
Medications	Medications' names	Medication (med_name)
Medication_forms	List of all medication forms	Medication(form)
Pharm_class_codes	List of pharmacological class codes	Medication (pharm_class_codes)
Pharm_subclass_codes	List of pharmacological subclass codes	Medication (pharm_subclass_code)

Table 5.1: Aggregate medications.

2. Step 2: join everything to patient table

Listing 5.3: Step 2: Join everything to patient table

```
SELECT
    p.pat_id,
    p.sex_abbr,
    p.ethnicity,
    p.country,
    p.state,
    p.seen_last_two_yrs_ind,
    p.marital_status,
    p.religion,
    COALESCE(m.medications, 'None') AS medications,
    COALESCE(m.medication_forms, 'None') AS
       medication_forms,
    COALESCE(m.pharm_class_codes, 'None') AS
       pharm_class_codes,
    COALESCE(m.pharm_subclass_codes, 'None') AS
       pharm_subclass_codes,

FROM arcus.patient p
LEFT JOIN Medications m ON p.pat_id = m.pat_id;
```

Execution process:

- Extracts patient demographic data from patient table.
- LEFT JOIN Medications:
  - Retrieves aggregated medication data for each patient.
  - Uses COALESCE() to replace NULL with 'None' if no medications exist

Final outputs:

Field name	Description	Source table
Pat_id	Patient ID	Patient
Sex_abbr	Sex (M/F)	Patient
Ethnicity	Patient's ethnicity	Patient
Country	Country of residence	Patient
State	State of residence	Patient
Seen_last_two_yrs_ind	Indicator if the patient was seen in the last 2 years	Patient
Marital_status	Marital status	Patient
Religion	Religion	Patient
Medications	List of all medications prescribed	Medication_order → medication
Medication_forms	List of medication forms	Medication
Pharm_class_codes	List of pharmacological class codes	Medication
Pharm_subclass_codes	List of pharmacological subclass codes	Medication

Table 5.2: Data dictionary for patient and medication information.

Regarding the patients' age, another query was made and added to the other output:

Listing 5.4: Patients' age query

```
WITH keys AS (
  SELECT
    original_value,
    SUBSTR(SPLIT(original_value, '_')[OFFSET(1)], 1, 15) AS
       key15
  FROM UNNEST([
    /* Here the patients ID are added one by one.
    .
    .
    . */
 ]) AS original_value
)

SELECT DISTINCT
  enc.pat_id,
  enc.encounter_id,
  proc.start_age,
  acc.acc_num,
  k.original_value   AS source_value
FROM `arcus.encounter` AS enc
JOIN `arcus.procedure_order` AS proc
  ON proc.encounter_id = enc.encounter_id
JOIN `arcus.procedure_order_accession` AS acc
  ON acc.proc_ord_id = proc.proc_ord_id

JOIN keys AS k
```

```
  ON SUBSTR(CAST(acc.acc_num AS STRING), 1, 15) = k.key15
;
```

As a result, although only age, medicines and gender factors were the ones used in the study, also others were exported in case they were of interest such as country, state or religion.

Demographic data research has been conducted to identify the factors affecting bone development, such as age, gender or ethnicity to make a descriptive statistical analysis.

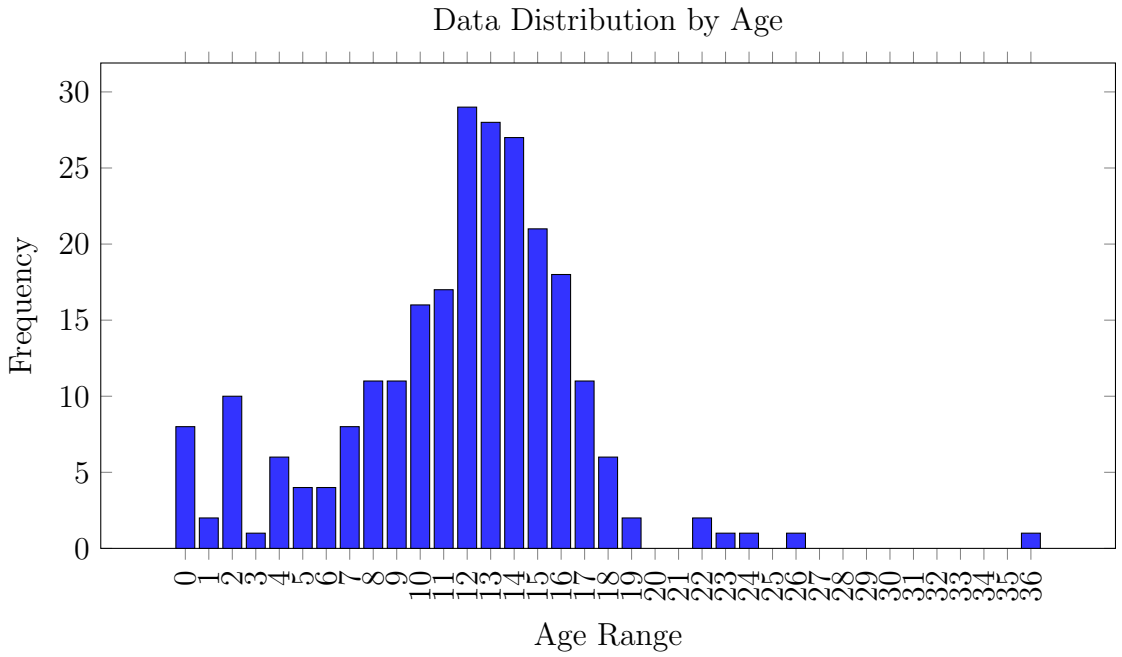

Figure 5.1: Distribution of People by Age.

5.2.2 Age Range

Regarding age, our aim was to find the age range of in which we wanted to divide our sample. After some research the following reasoning was developed. Ideally, these are the age ranges wished:

1. Infancy and early childhood (0-5):
   In this period of life happens a rapid longitudinal bone growth, particularly in the first two years [12]. It has a strong dependence on nutritional factor, as endocrine control overgrowth is still developing [13]. Growth rates slow down after infancy [14].
   No significance sex differences. [13] [12]

Age range (0-5): 0-2; 2-4 years.

As the two first years are the most remarkable ones, grouping them together is reasonable as some children have a more remarked growth in the first year and others in the second one.

2. Mid-childhood (5-10y)
   Relatively stable and steady growth phase compared to infancy and puberty [15]. Gradual increase in adrenal androgens initiating adrenarche, but minimal direct effects on growth plates yet [13]. GH and IGF-1 Remain dominant as in infancy and early childhood, though their effects are less pronounced [12] [16]. Growth remains steady and similar between boys and girls [13] [15]

Age range (5-10): 5-7; 8-9 years.

3. Pre-puberty and early pubertal growth (10-14y)
   Pubertal growth spurt begins [17] [18] [19]. In this period, oestrogen plays a major role in both males and females. In males, the remarkable bone growth is 12-14 years, and in females between 10-12 years. Being longer and more intense in male [15]. Girls peak is around 11-12 years, while boys is around 13-15 years. [17] [18] [19]

Age range (10-14): 10-12; 13-14 years.

4. Late puberty and epiphyseal closure (14-18y)
   Growth plate senescence accelerates, leading to gradual closure [20] [21]. Height velocity declines as growth plates narrow and eventually fuse [17] [22]. Girls closing growth begins around 16 years. [21]. In girls, the growth plate fusion occurs earlier, around 14-16 years and complete by 16-18 years. In boys, fusion begins in 16-18 years and finishes by 21 years.[23]. After 21, both males and females have undergone growth plate fusion, and no further longitudinal growth occurs.

Age range: 14-15; 16-18; 19-21; 22-+... years

The CHOP has provided us with a total of 246 patients, from which 99 were females and 147 males, following this age distribution:

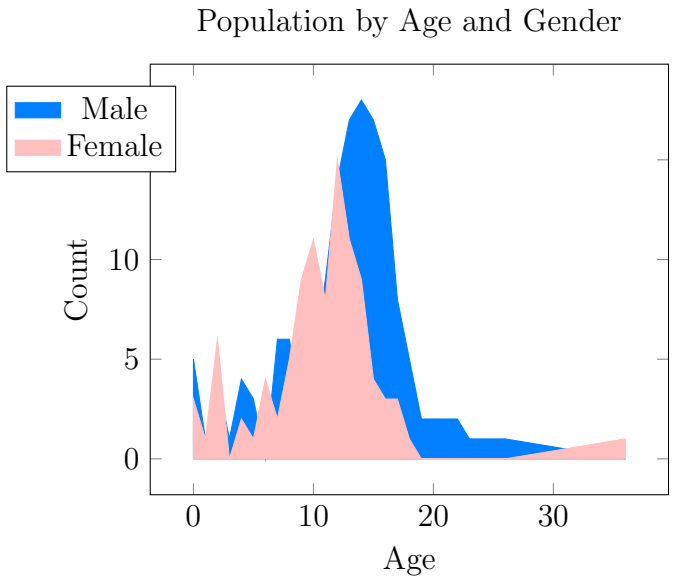

Figure 5.2: Distribution of People by Age and Gender.

Our aim is to divide the study into each gender and age ranges. Summarized tables have been created to visualize different possible options regarding our sample, being the first row the ideal. What is more, each table have to be doubled due to gender differences.

Table 5.3: Distribution of Samples Across Different Age Ranges

Samples per range	**Age ranges**										**N total**
	0-2	**3-4**	**5-7**	**8-9**	**10-12**	**13-14**	**14-15**	**16-18**	**19-21**	**22-+**	
N*30	0-2	3-4	5-7	8-9	10-12	13-14	14-15	16-18	19-21	22-+	300(*2)
N*30	0-2	3-4	5-7	8-9	10-12	13-14	14-15	16-18	19+		270(*2)
N*30	0-2	3-4	5-9		10-12	13-14	14-15	16+			210(*2)
N*30	0-4		5-9		10-12	13-14	14-15	16+			180(*2)

This was the desired age ranges.

These possible age ranges were sent to a specialist so ensure our results. Based on his opinion, other factors are also important.

5.2.3 Ethnicity

Factors such as ethnicity, diet and genes make an important difference in bone's development and shape. However, our database only shows the options of Hispanic or Latino, Non-Hispanic or Non-Latino, Refused, Unknown, Other where

non-Hispanic or non-Latino represents the vast majority:

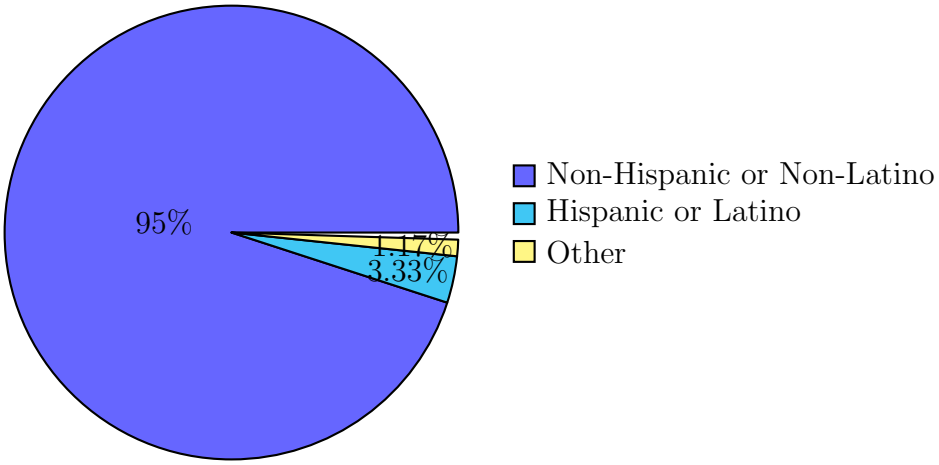

Unfortunately, not enough data is registered in order to have this factor into account.
The thickness of the tibia should be measured in the diaphysis (the central and longest part of the tibia). It would be of special interest to analyze the saturation of the development curve as well as its' value. It is expected to be before and thinner in women.

5.2.4 Medication

Medicines are also a decisive influencing factor. There are harmful medications that affect bone development. Patients taking these medications need to be removed from the study, as their bone development may have been affected. The list of the harmful medications is:

- Potassium phosphate
- Heparin
- Etoposide
- Temsirolimus
- Carboplatin
- Ravulizumab-cwvz
- Etomidate
- Gemcitabine

- Calcium gluconate
- Oxaliplatin
- Doxorubicin/cisplatin/mitomycin-C
- Cisplatin
- Dexrazoxane
- Vincristine
- Furosemide
- Metolazone
- Ifosfamide-mesna
- Hydrocortisone
- Doxorubicin
- TPN child
- Dexamethasone
- Hydrocortisone sodium succinate
- Bumetanide

After deleting from the database the patients with any of these harmful medicines, the diagrams show our new database:

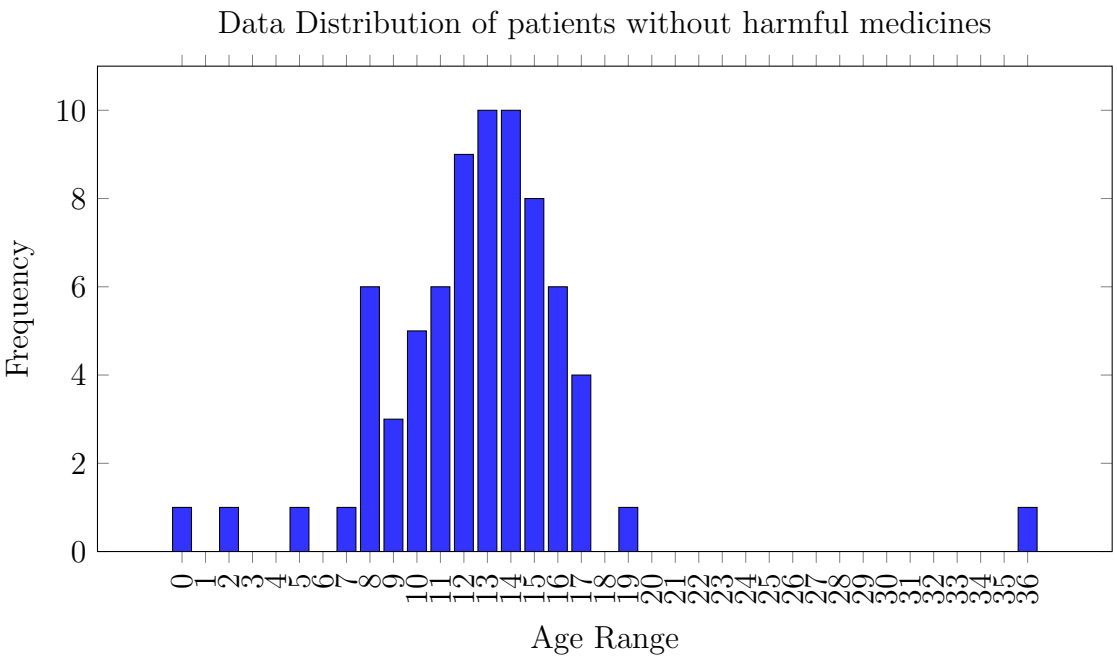

Figure 5.3: Distribution of People without Harmful Medicines by Age

And its' distribution by gender:

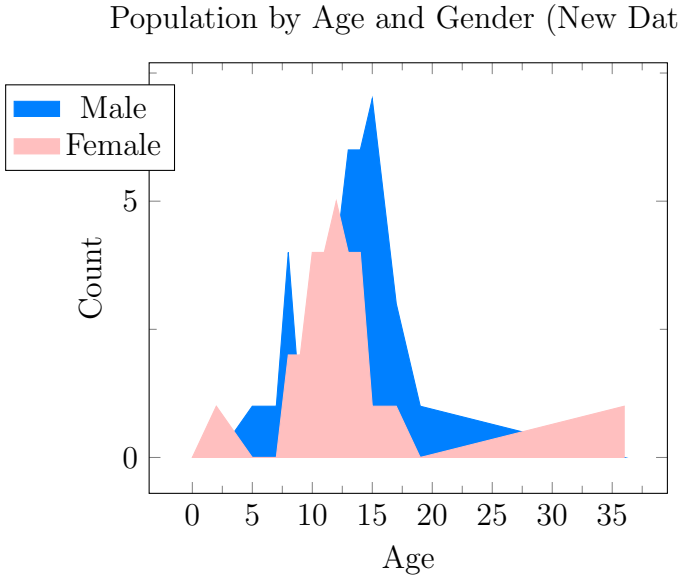

Figure 5.4: Distribution of People with Not-Harmful Medicines by Age and Gender.

5.3 Coding

After having clarified the age ranges and demographic factors that were going to be studied, the selected bones needed to be revised and some edited to eliminate the non-desired objects with high HU, such as the stretcher or a prosthesis. Deleting the studies carried out on the same day or within a relatively short period of time resulted in the database containing 246 patients, from whom only 73 patients could be used in our study, as we removed those with harmful medicines. After editing the files and running the code, because of broken or abnormal bones, the final statistical analysis was carried out with 60 files. The discarded bones are specified in Annex II.

Due to the deletion and discarding of patients, the database in which the algorithm is to be applied has been significantly reduced. Therefore, to avoid a biased study, the desired age range cannot be used and must be reorganized. For the final age ranges, three factors will be considered.
Firstly, the bone development significance along each age. Secondly, the opinion of experts and, thirdly, the number of files there are of each range.
The bones will be divided into the following age range:

Age range	Files
0-9	10
10-11	10
12-13	10
14-15	15
16-17	11

Table 5.4: Number of Files by Age Range.

Once the final database containing the preprocessed and corrected bone images was prepared, the processing pipeline was executed. The first step involved running the script `generateSTL.py`, which generated a three-dimensional STL representation for each bone in the dataset. All resulting 3D models are included in Annex III for reference.

To ensure consistent alignment and orientation across all samples, a reference bone was selected. This reference model corresponds to an 11-year-old male and served as the standard against which all other bones were registered during the alignment phase.

Figure 5.5: Reference Bone: 11-year-old male

As its name suggests, the reference bone was used as the standard model against which all other bones in the dataset were aligned and oriented.

By executing the script `referenceBone.py`, an orientation vector was generated based on the geometry of the reference model. Additionally, the thickness contours and profile sections of the bone were extracted and saved as output files. A color-coded 3D contour model was also generated, where different colors represent varying levels of bone density, providing a visual representation of cortical thickness distribution.

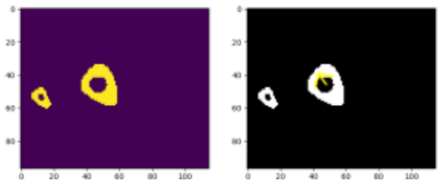

Figure 5.6: Reference vector

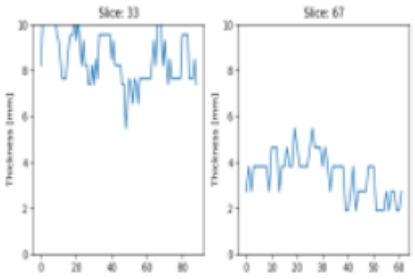

Figure 5.7: Reference profiles

Figure 5.8: 3D contour

Next, the `correctionsThickness.py` script was reviewed and executed. As previously described, this script aligns and orients each bone in the dataset with respect to the reference model, ensuring consistency across all samples.

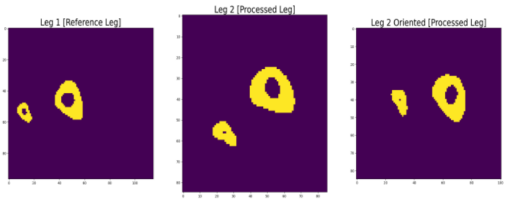

Figure 5.9: Example of alignment and orientation

Some of them needed to be corrected as they were from the other leg (left-/right) or were oriented/aligned in the opposite direction. To do this, the code `cT_Retake.py` is executed, specifying the files that need to be corrected.

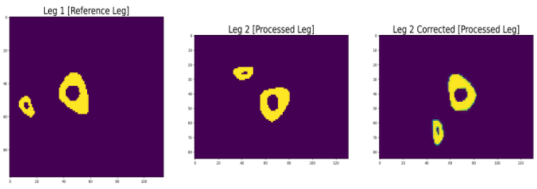

Figure 5.10: Example of opposite orientation

As an output, it gives the thickness and profiles of every bone as NumPy and Pickled files respectively. These are the files with which we will do our analysis.

5.4 Statistical Analysis

To conduct a statistical study on the evolution of cortical tissue in children, two studies will be carried out: one comparative by age range and another by age and gender. Also, they will be made for the whole bone and the diaphysis, the zone of major interest in bone growth. Two methods will be used separately to make this analysis and later on compare the results; Pickled (profiles) and NumPy (matrices) files.

5.4.1 Whole bone analysis

For this part of the study, the bones that only had the diaphysis (the long part of the bone) and not the epiphysis (the ends) were discarded.

Matrices

To export the data from the NumPy files to calculate the average of each bone, the following Python code was created:

```
1  import numpy as np
2  import glob
3  import os
4  import csv
5
6  # Folder containing the .npz files
7  folder_path = '/mnt/arcus/lab/users/corpasgonm/
       corticalMeasurement/done/out_10to11/thickness/'
8
9  # Get all .npz files in the folder
10 npz_files = glob.glob(os.path.join(folder_path, '*.npz'))
11
```

```
# Prepare the results
results = []

for file_path in npz_files:
    data = np.load(file_path)
    array = data['arr_0']
    avg = np.mean(array)
    filename = os.path.basename(file_path)
    results.append([filename, avg])

# Write results to a CSV
output_csv = os.path.join(folder_path, 'averages.csv')
with open(output_csv, mode='w', newline='') as f:
    writer = csv.writer(f)
    writer.writerow(['Filename', 'Average'])
    writer.writerows(results)

print(f"Averages saved to: {output_csv}")
```

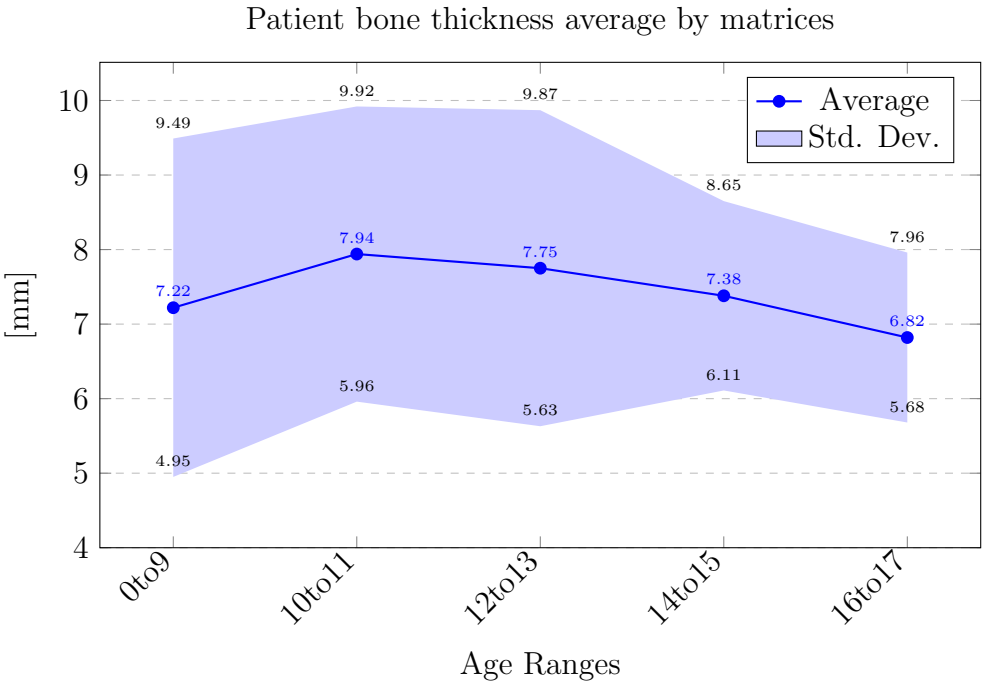

Figure 5.11: Bones' thickness average with standard deviation.

As shown in the graphic fig. 5.11, bone thickness increases until the age of 10-11 years; right when spurt begins, and decreases thereafter.

For the comparison by gender, the distribution of the database is the following:

Age range	F	M
0 to 9	4	6
10 to 11	7	3
12 to 13	6	8
14 to 15	5	10
16 to 36	3	8

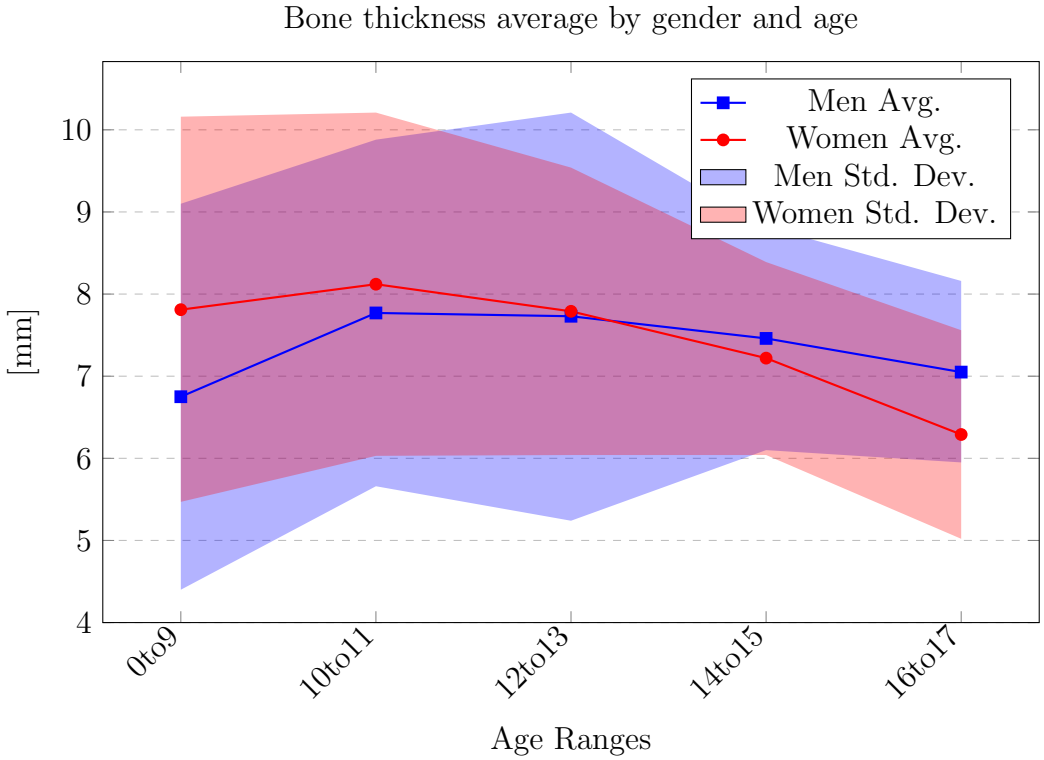

Figure 5.12: Bone thickness average by gender and age by matrices

The comparison between females and males shows that females' bone thickness decreases significantly more at the age of 16-17 than males.

Profiles

The thickness was also calculated by the Pickled files. Here is an example of the 9 profiles a bone is divided into:

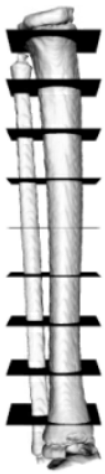

Figure 5.13: Bone divided in profiles

To extract the data, this code was executed in Python:

```
import pickle
import numpy as np
import csv
import os
import glob

# Folder containing the .pkl files
folder_path = '/mnt/arcus/lab/users/corpasgonm/
   corticalMeasurement/done/out_16to36.1/profiles/'

# Get all .pkl files in the folder
pkl_files = glob.glob(os.path.join(folder_path, '*.pkl'))

# Prepare results list
results = []

# Process each .pkl file
for file_path in pkl_files:
    filename = os.path.basename(file_path)

    with open(file_path, 'rb') as f:
        data = pickle.load(f)

    for key, values in data.items():
        avg = np.mean(values)
```

```
        results.append([filename, key, avg])

# Write to a single CSV file
output_csv = os.path.join(folder_path, 'all_averages.csv')
with open(output_csv, 'w', newline='') as csvfile:
    writer = csv.writer(csvfile)
    writer.writerow(['Filename', 'Key', 'Average'])
    writer.writerows(results)

print(f" Averages from all .pkl files saved to: {output_csv}
    ")
```

As a result, we obtaine this thickness development:

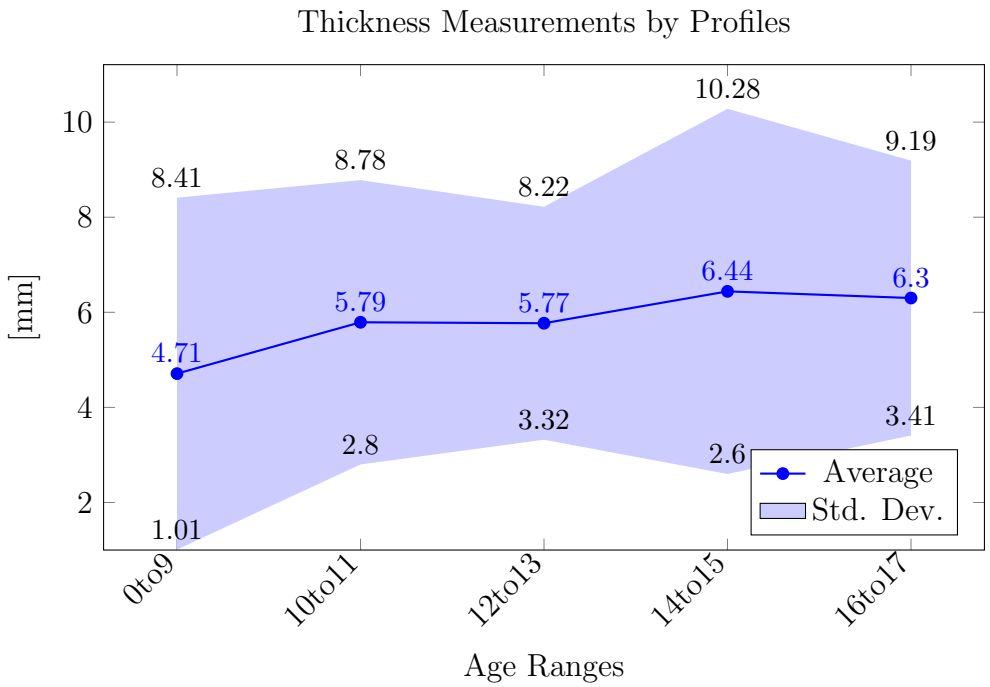

Figure 5.14: Thickness development by profiles, with standard deviation.

By gender:

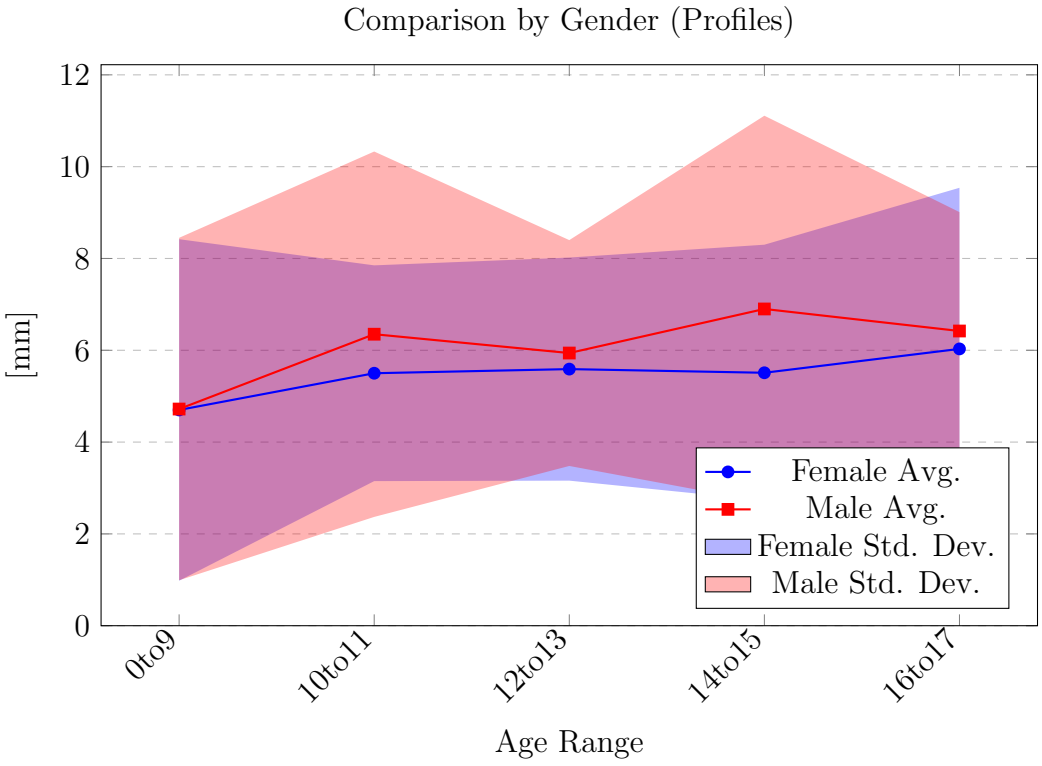

Figure 5.15: Thickness development by profiles and gender, with standard deviation bands.

Comparison between the two methods

To compare both methods and check reliability a combination of statistical analyses is done.

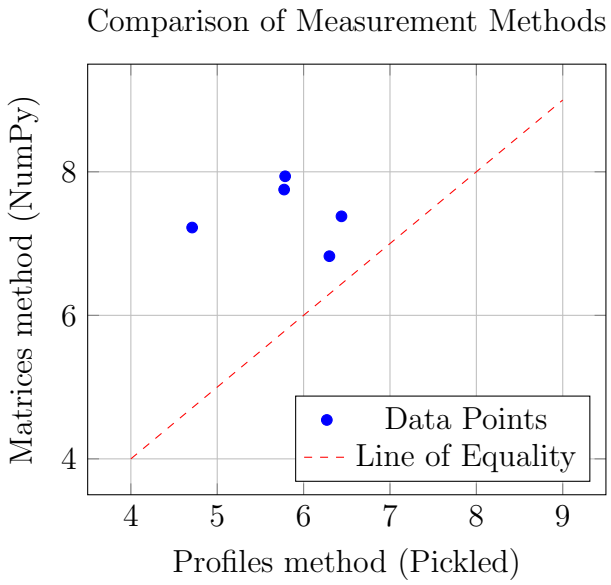

Figure 5.16: Scatterplot comparing bone thickness measurements.

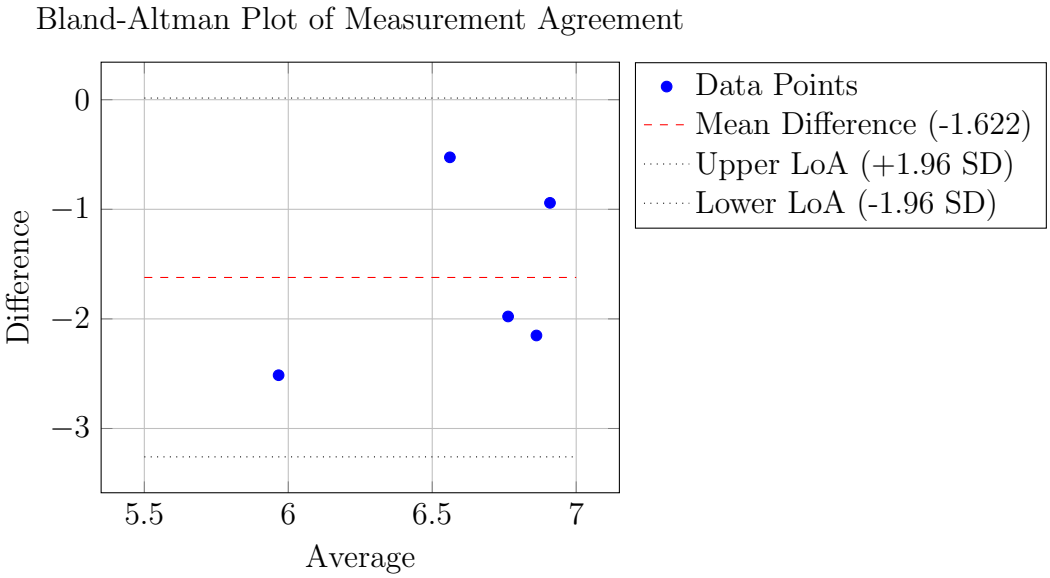

Figure 5.17: Bland-Altman plot.

The scatterplot gives a visual check. As the points do not fall on the y=x line, both methods do not agree completely. The Bland-Altman Plot is used to check whether the study is biased or not. The two main points to analyze the two methods compared are:

- Bias: If the mean is far from zero, it indicates a systematic bias. The dashed red line is the mean difference, which is -1.622. This indicates a significant systematic bias, where the profiles method consistently measures about 1.62 units lower than the matrices method.

- Limits of Agreement: The dotted black lines show the range where 95% of differences are expected to fall. This range is from -3.259 to 0.015.

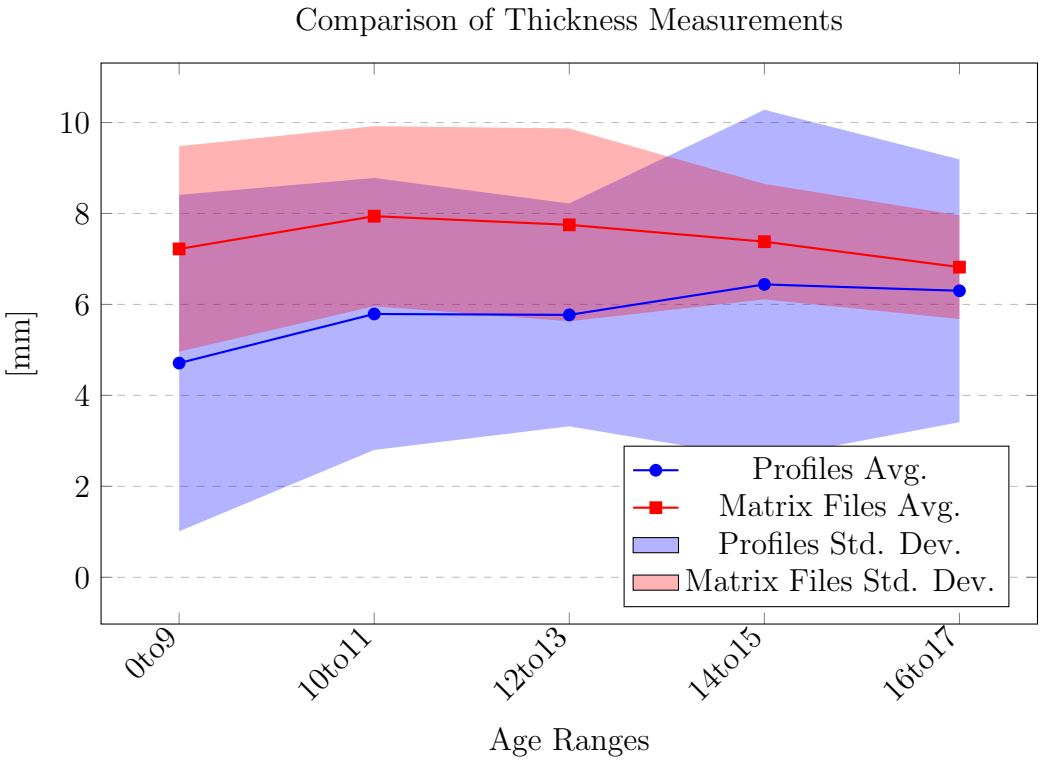

Figure 5.18: Comparison of thickness measurements from profiles and matrices.

To conclude, the two methods used to calculate the whole thickness of each bone, are not in agreement. Probably the reason of this is that the matrix takes into account all the epiphysis while the Pickled takes only part of it. At the epiphysis the bone thickness is more remarked, so it affects notably to the final result of the averages.

Comparison by gender:

Female

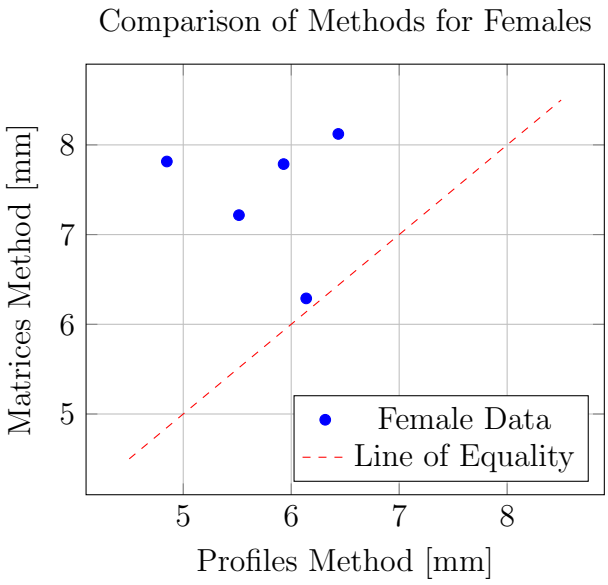

Figure 5.19: Scatterplot comparing the two measurement methods for female data.

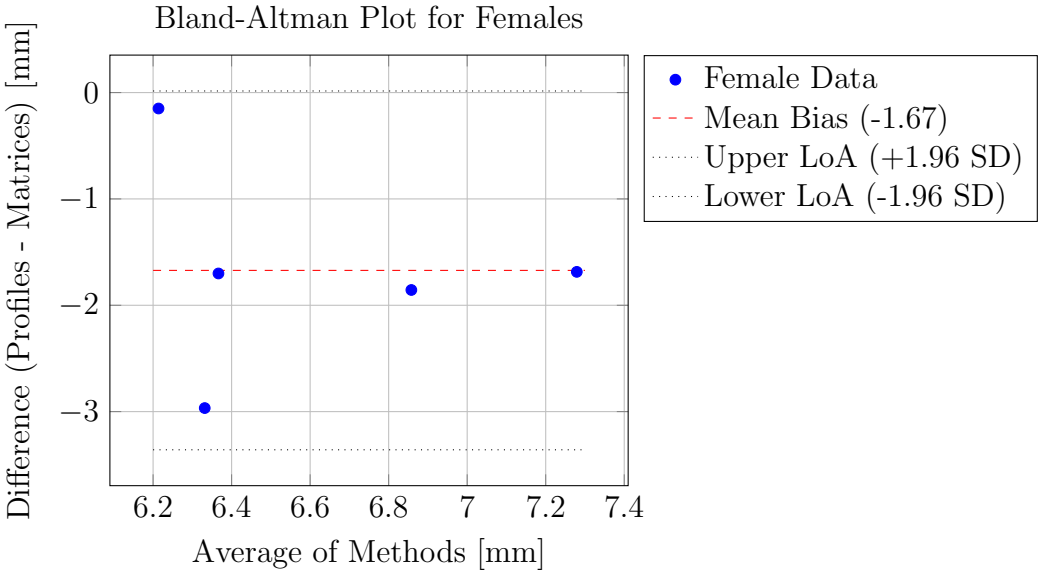

Figure 5.20: Bland-Altman plot for female data comparing the profiles and matrices methods.

Male:

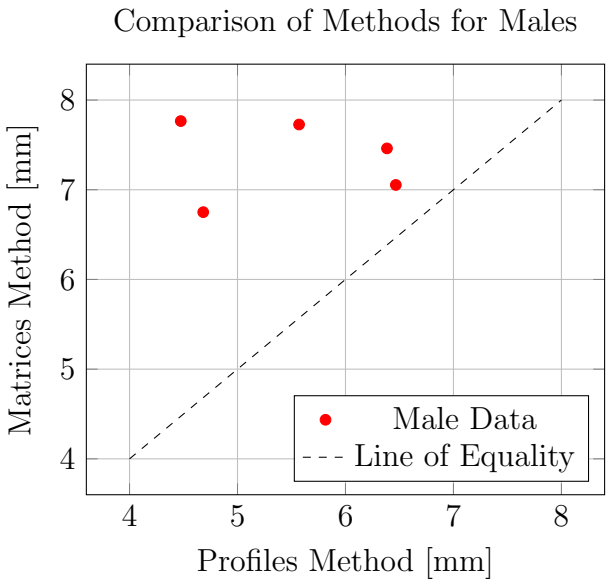

Figure 5.21: Scatterplot comparing the two measurement methods for male data.

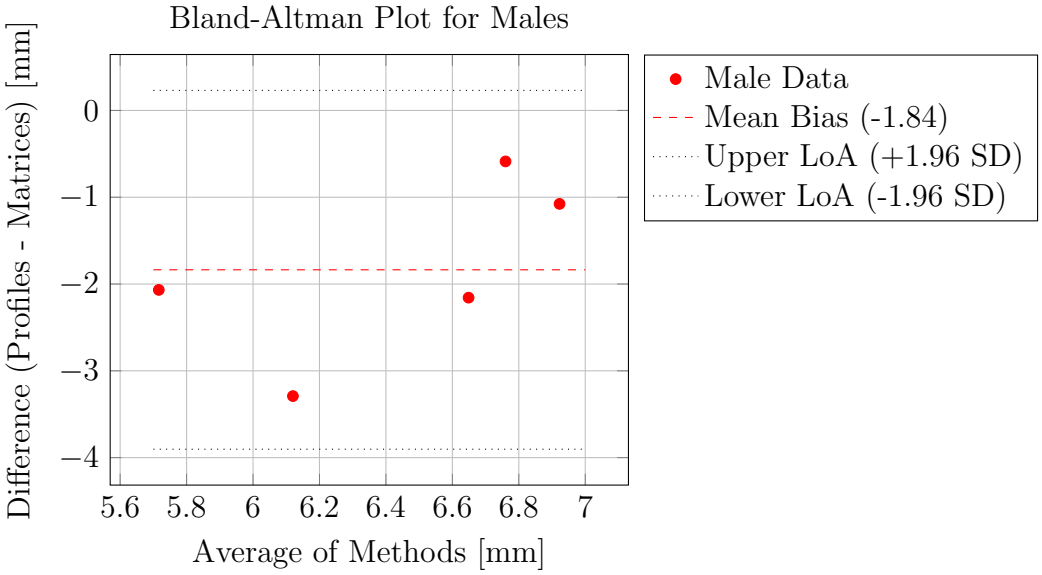

Figure 5.22: Bland-Altman plot for male data comparing the profiles and matrices methods.

For females, the profiles method measures, on average, 1.67 mm lower that the matrices one, while for males is 1.84 mm lower. Thus, the male sample is slightly more biased than the female.

5.4.2 Central area analysis

As the thickness of the tibia should be measured in the diaphysis, the centered zone of the bone, both in the Pickled and NumPy files, that zone will be extracted and analyzed to compare the results and see the veracity.

Matrices

On the other hand, to compare results and check reliability, with the matrix of the NumPy files, another analysis was made. The interest zone of the bone is from 40% to 60% of the bone length. The code used to extract it was the following:

```
    import numpy as np
import os
from pathlib import Path
import csv

# Ruta a la carpeta que contiene los archivos .npz
carpeta = Path('/mnt/arcus/lab/users/corpasgonm/corticalMeasurement/done/out_16to36.2/thickness/')

# Buscar todos los archivos .npz
archivos_npz = list(carpeta.glob('*.npz'))

# Lista para guardar resultados
resultados = []

for archivo in archivos_npz:
    print(f"Procesando: {archivo.name}")

    data = np.load(archivo)

    if 'arr_0' not in data.files:
        print(f"    'arr_0' no encontrado, se omite {archivo.name}")
        continue

    espesores = data['arr_0']

    # Confirmar que es 3D
    if espesores.ndim != 3:
        print(f"    El array no es 3D, se omite {archivo.name}")
        continue
```

```
30
31      # Calcular cortes del 40%-60%
32      n = espesores.shape[0]
33      start = int(0.4 * n)
34      end = int(0.6 * n)
35      zona_media = espesores[start:end, :, :]
36
37      # Calcular promedio
38      promedio = np.mean(zona_media)
39      resultados.append([archivo.name, promedio])
40      print(f"   Promedio zona media: {promedio:.4f}")
41
42  # Guardar resultados en un archivo CSV
43  csv_path = carpeta / 'promedios_zona_media.csv'
44  with open(csv_path, mode='w', newline='') as f:
45      writer = csv.writer(f)
46      writer.writerow(['archivo', 'promedio_zona_media'])
47      writer.writerows(resultados)
48
49  print(f"\nTodos los promedios guardados en: {csv_path}")
```

As a result:

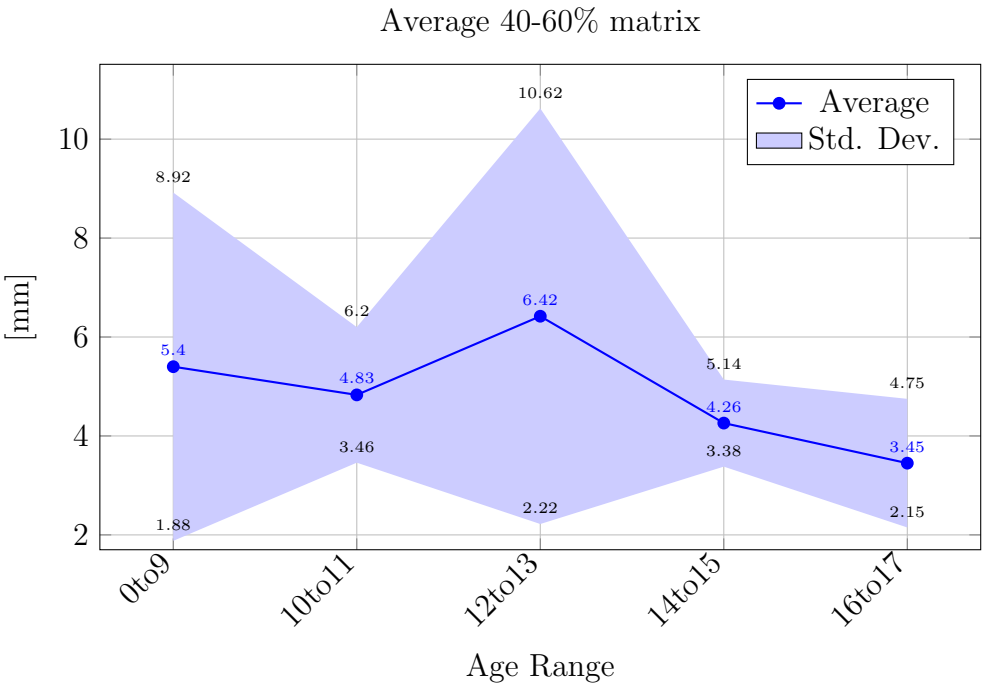

Figure 5.23: Bone Thickness' Average of 40-60% Matrix for Age Ranges.

And by gender:

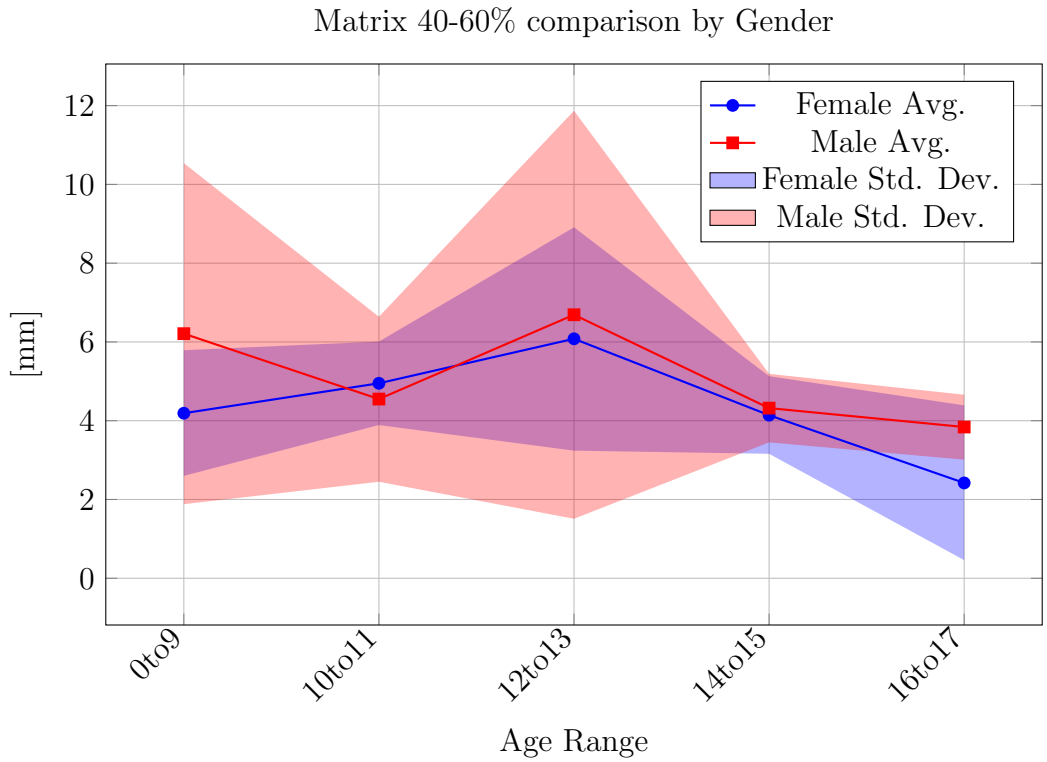

Figure 5.24: Bone Thickness' Average of 40-60% Matrix for Age Ranges and Gender.

Profiles

In the profiles, the one of interest, as the bone is divided into 9 profiles, in the vast majority of the cases, is profile 5. For those bones that are not complete, deeper research needs to be done in order to analyze which profile corresponds to the central one. [1] The average of each age range and gender is the following:

[1] See Annex II

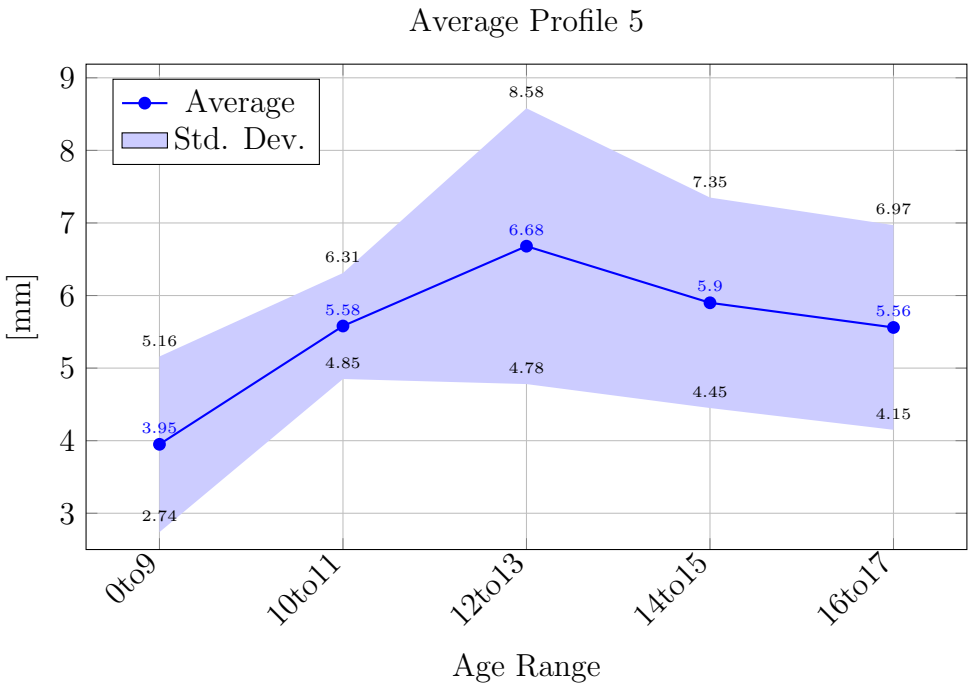

Figure 5.25: Bone Thickness' Average of Profile 5 for Age Ranges.

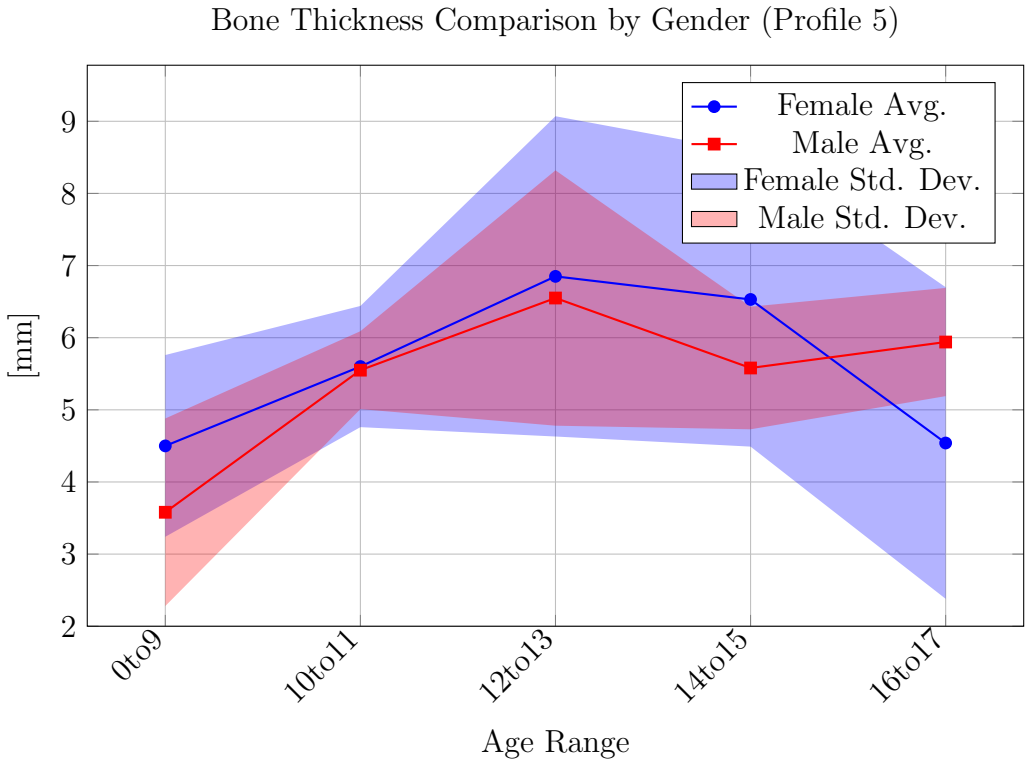

Figure 5.26: Average bone thickness of profile 5 by Gender and Age.

Comparison

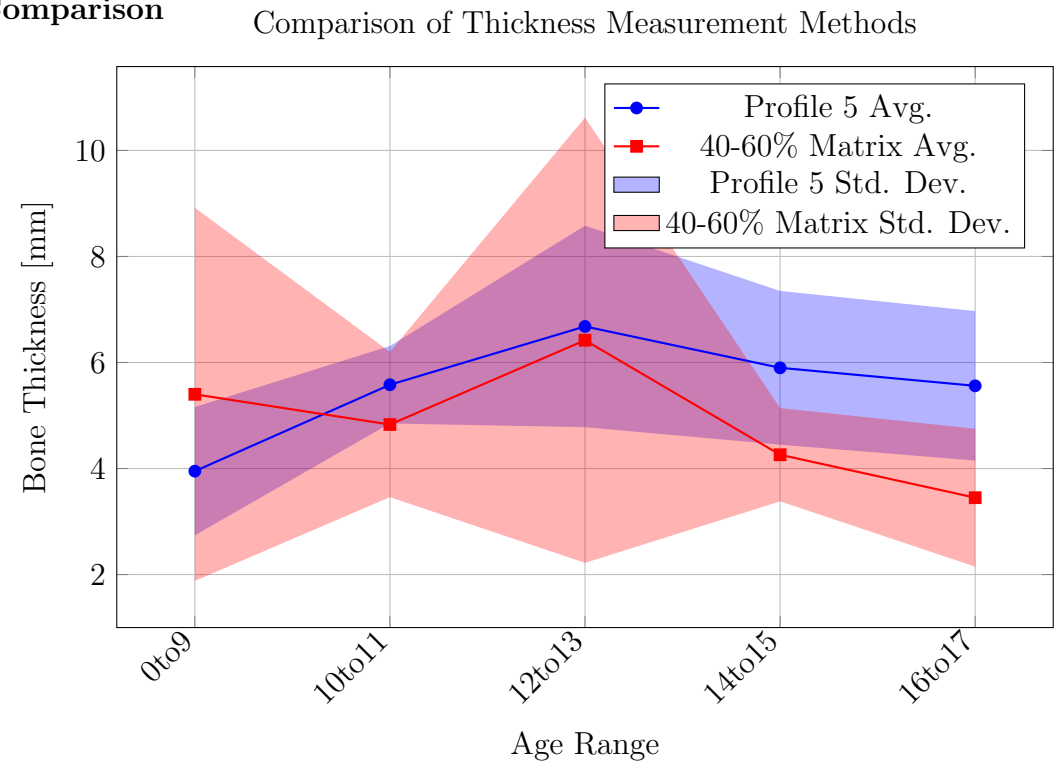

Figure 5.27: Central Bone Thickness Measurements from the Different Methods.

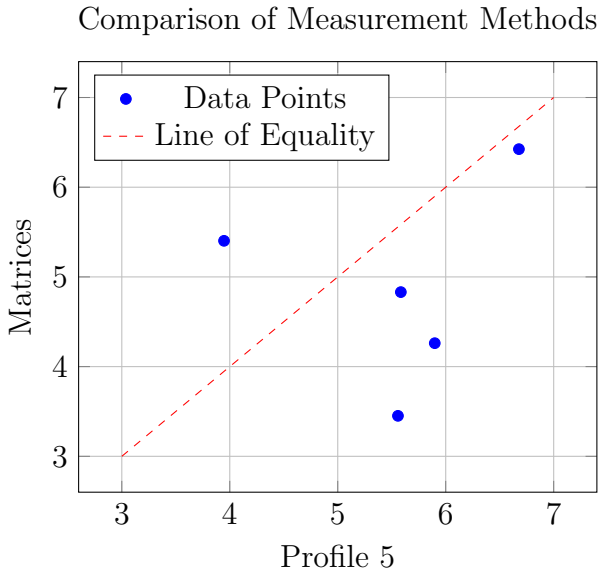

Figure 5.28: Scatterplot Comparing the Two Methods.

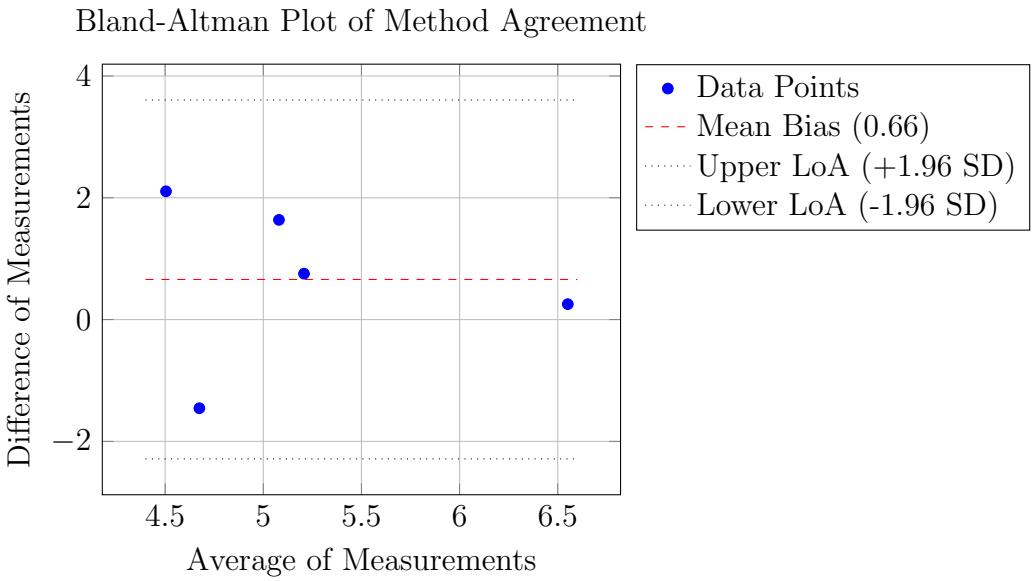

Figure 5.29: Bland-Altman plot comparing the two methods.

As it was expected, a better result is obtained from the center bone analysis, as the mean bias is closer to zero. As explained before, the reason for this is probably due to not including the epiphysis.

By gender:

Female

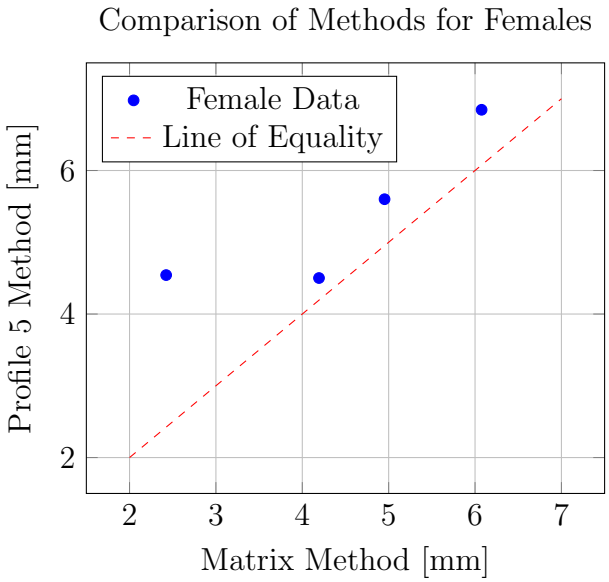

Figure 5.30: Scatterplot Comparing the Two Methods for Female.

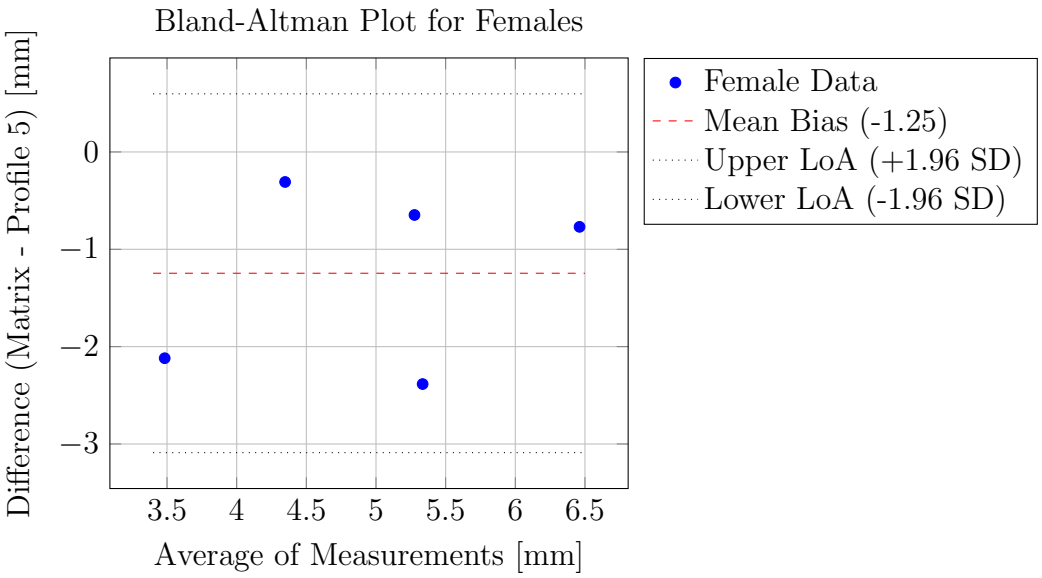

Figure 5.31: Bland-Altman plot for female data.

Male

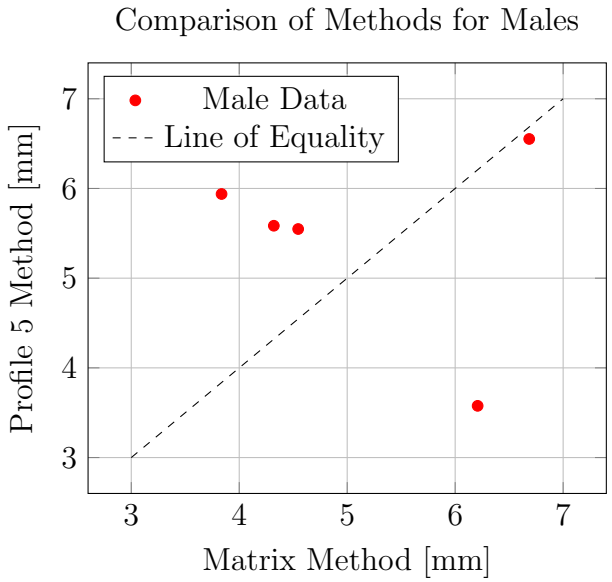

Figure 5.32: Scatterplot comparing the two measurement methods for male data.

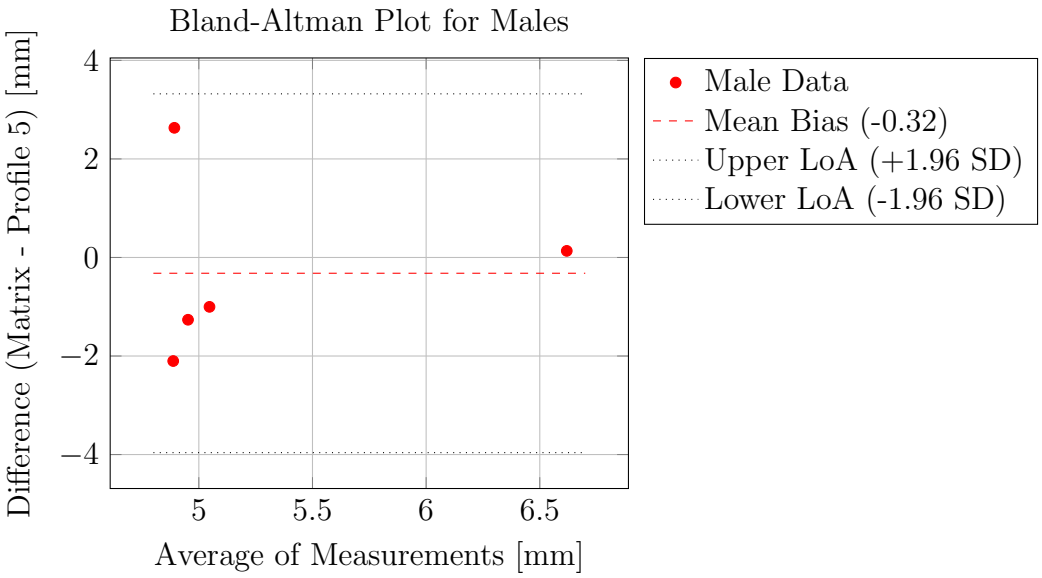

Figure 5.33: Bland-Altman plot for Male.

For males, the bias is much smaller than for females (0.32mm lower compared to 1.25 mm lower respectively). However, the limits of agreement are wider in male, suggesting the methods have less consistent agreement for this group.

Chapter 6

Results

6.1 Whole bone analysis

The average thickness per age range is:

- By the matrices files:

Table 6.1: Matrix data: Average and Standard Deviation by Age Range

Age Range	**(Average ± Std. Dev.)**
0–9	$0.072233845 \pm 0.022634562$
10–11	$0.079376211 \pm 0.019788901$
12–13	$0.077524191 \pm 0.021206980$
14–15	$0.073795757 \pm 0.012666548$
16–17	$0.068241878 \pm 0.011415286$

- By profiles (Pickled files):

Table 6.2: Profile Data: Average and Standard Deviation by Age Range

Age Range	**(Average ± Std. Dev.)**
0–9	$0.04709489 \pm 0.03703337$
10–11	$0.05786274 \pm 0.02995765$
12–13	$0.05774529 \pm 0.02445645$
14–15	$0.06438357 \pm 0.03843329$
16–17	$0.06298521 \pm 0.02886544$

Divided by gender:

Female

- By the matrices files:

Table 6.3: Matrix Data: Female Average and Standard Deviation by Age Range

Age Range	**(Average ± Std. Dev.)**
0–9	$0.07814899 \pm 0.02341446$
10–11	$0.08122163 \pm 0.02087747$
12–13	$0.07785924 \pm 0.01749479$
14–15	$0.07217002 \pm 0.01179605$
16–17	$0.06288732 \pm 0.01266442$

- By the profiles (Pickled files):

Table 6.4: Profile Data: Average and Standard Deviation by Age Range

Age Range	**(Average ± Std. Dev.)**
0–9	$0.04695778 \pm 0.03722246$
10–11	$0.05504478 \pm 0.02350271$
12–13	$0.05591126 \pm 0.02433114$
14–15	$0.05512250 \pm 0.02785100$
16–17	$0.06026203 \pm 0.03517676$

Male

- By matrices files:

Table 6.5: Matrix Data: Male Average and Standard Deviation by Age Range

Age Range	**(Average ± Std. Dev.)**
0–9	$0.06750173 \pm 0.02346250$
10–11	$0.07765542 \pm 0.02112060$
12–13	$0.07727291 \pm 0.02482812$
14–15	$0.07460863 \pm 0.01362094$
16–17	$0.07053669 \pm 0.01102366$

- By the profile (Pickled files)

Table 6.6: Profile Data: Average and Standard Deviation by Age Range

Age Range	**(Average ± Std. Dev.)**
0–9	$0.04720457 \pm 0.03730205$
10–11	$0.06349866 \pm 0.03982385$
12–13	$0.05942932 \pm 0.02462984$
14–15	$0.06901411 \pm 0.04213603$
16–17	$0.06415228 \pm 0.02593336$

6.2 Central area analysis

Results

The average thickness in the central area per age range is:

- By the matrices files:

Table 6.7: Matrix Central Area Data: Average and Standard Deviation by Age Range

Age Range	**Value (Average ± Std. Dev.)**
0–9	$0.05402276 \pm 0.03516125$
10–11	$0.04830593 \pm 0.01374039$
12–13	$0.06424361 \pm 0.04199897$
14–15	$0.04261163 \pm 0.00878648$
16–17	$0.03451148 \pm 0.01297151$

- By the profiles (Pickled files):

Table 6.8: Profile 5 data: Average and Standard Deviation by Age Range

Age Range	**(Average ± Std. Dev.)**
0–9	$0.0394672528 \pm 0.0121429999$
10–11	$0.0558441179 \pm 0.0073493251$
12–13	$0.0667799709 \pm 0.0190371120$
14–15	$0.0589860648 \pm 0.0145516797$
16–17	$0.0555763184 \pm 0.0141165365$

And divided by gender:

Female

- By the matrices files:

Table 6.9: Matrix Central Area Data: Average and Standard Deviation by Age Range

Age Range	**(Average ± Std. Dev.)**
0–9	$0.04193496 \pm 0.01596511$
10–11	$0.04952602 \pm 0.01061409$
12–13	$0.06075965 \pm 0.02836272$
14–15	$0.04142610 \pm 0.00983758$
16–17	$0.02423890 \pm 0.01964776$

- By the profiles (Pickled files):

Table 6.10: Profile 5 Data: Average and Standard Deviation by Age Range

Age Range	**Value (Average ± Std. Dev.)**
0–9	$0.0450180508 \pm 0.0126424200$
10–11	$0.0560004113 \pm 0.0084298513$
12–13	$0.0684626542 \pm 0.0222145045$
14–15	$0.0652695130 \pm 0.0203575592$
16–17	$0.0454278770 \pm 0.0216354294$

Male

- By the matrices files:

Table 6.11: Matrix Data: Average and Standard Deviation by Age Range

Age Range	**(Average ± Std. Dev.)**
0–9	$0.06208130 \pm 0.04333144$
10–11	$0.04545903 \pm 0.02092652$
12–13	$0.06685658 \pm 0.05179797$
14–15	$0.04320439 \pm 0.00871256$
16–17	$0.03836369 \pm 0.00823961$

- By the profiles (Pickled files):

Table 6.12: Profile 5 Data: Average and Standard Deviation by Age Range

Age Range	**(Average ± Std. Dev.)**
0–9	$0.0357667208 \pm 0.0129500716$
10–11	$0.0554794333 \pm 0.0054391579$
12–13	$0.0655179585 \pm 0.0176511042$
14–15	$0.0558443407 \pm 0.0085457068$
16–17	$0.0593819839 \pm 0.0074599285$

This project aimed to evaluate an automated pipeline for measuring cortical bone thickness in pediatric tibial CT images. The final implementation consisted of two primary approaches: one using matrices generated from the segmentation output, and another using profile-based pickled data representing specific bone cross-sections. Both methods were applied to a dataset of CT scans spanning ages 0 to 17, with additional stratification by sex and central anatomical region.

The results provide a nuanced view of the effectiveness and limitations of the implemented methods. In line with physiological expectations and literature, cortical thickness is generally expected to increase during childhood and early adolescence, particularly around the onset of puberty. This pattern was partially reflected in the *profile-based* data, where cortical thickness increases from early childhood and plateaus or slightly decreases around ages 14–17, likely due to growth plate closure or sampling noise.

Conversely, the *matrix-based* measurements often showed a counterintuitive trend—thickness decreasing with age. This discrepancy was especially pronounced in the female subgroup and in the central region measurements. After a careful review of possible causes, three main hypotheses were proposed:

- The image quality and resolution—particularly in pediatric imaging—may hinder precise cortical boundary detection.
- Sample bias and class imbalance, especially with small cohort sizes in older age groups, may distort average values.
- The current dataset may be insufficient in size and diversity to generalize biological trends confidently.

Among these, dataset limitations appear to be the most plausible cause. The matrix pipeline may also be more sensitive to segmentation inaccuracies, especially when estimating thickness near the periosteal and endosteal borders.

Despite the inconsistencies, the profile method provided results that are both quantitatively and biologically more coherent. When analyzed by sex, the male group generally showed slightly higher average thickness values than females—another trend supported by existing anatomical literature. Standard deviations remained relatively high across both approaches, particularly in the profile method, indicating inter-individual variability and potential segmentation noise.

Final Remarks

Although not all results strictly followed the expected biological patterns, the project successfully demonstrates the feasibility of automating cortical thickness analysis in pediatric bone imaging. The profile-based method, in particular, shows promise for future development. With further refinement and validation, this approach could become a valuable tool for studying bone growth, diagnosing developmental abnormalities, or evaluating treatment effects in pediatric populations.

Chapter 7

Conclusions and future work

With our database, sixty bones were processed, from which the following data were extracted:

- Bone masks and labeling.
- Alignment and orienting vectors.
- 3D bone representation.
- Leg side (right / left)

Average bone thickness in each age range was calculated based on the measures of all the files, with a standard deviation. However, the results comparing both methods implied, were not too conclusive. Deeper research will need to be done to understand the reason for these results.

Future Work

The outcomes of this project lay the groundwork for multiple avenues of future research and clinical application. As the field of medical image analysis continues to evolve, the methodology developed here can be further extended and refined to improve both technical performance and clinical relevance.

Technical Improvements and Expansion

- **Dataset Expansion:** Increasing the number of CT scans across all age ranges and ensuring balanced representation by sex, ethnicity, and health status would significantly improve the statistical validity of the findings. A larger dataset would also enhance the robustness of any machine learning models developed in future iterations.

- **Integration of Deep Learning Models:** Replacing classical segmentation techniques with advanced convolutional neural networks (CNNs)—such as U-Net or Attention U-Net—could lead to more accurate and consistent segmentation, especially in low-resolution or noisy images. These models can also generalize better across anatomical variability.

- **Validation with Clinical Experts:** A crucial next step is to validate the automatically generated measurements against annotations or measurements performed by expert radiologists. This comparison would establish the algorithm's clinical credibility and its potential for deployment in real-world diagnostic settings.

- **Temporal and Longitudinal Studies:** Expanding from cross-sectional to longitudinal studies would enable tracking of cortical thickness changes within the same individuals over time. This could provide deeper insights into bone development, disease progression, or the effects of specific treatments.

Clinical Applications and Real-World Use

- **Surgical Planning and 3D Modeling:** The segmentation output could be used to generate accurate 3D reconstructions of bones. These models could then be printed in color, showing bone density variations, which would greatly assist surgeons in preoperative planning, especially in complex pediatric or orthopedic cases.

- **Disease Detection and Monitoring:** Automated analysis of cortical thickness could contribute to early detection of bone diseases such as osteosarcoma, osteoporosis, or hyperparathyroidism. Monitoring changes in cortical structure over time could also be useful in evaluating the progression of these diseases or the response to treatment.

- **Treatment Personalization and Monitoring:** By integrating cortical thickness metrics with patient history, clinicians could better tailor treatments and assess their effectiveness over time. This could be particularly relevant in therapies involving calcium supplementation, growth hormone treatments, or post-surgical recovery assessments.

Exploratory and Demographic Research Directions

- **Bone Length vs. Thickness Correlation:** Measuring the longitudinal length of the tibia and analyzing its relationship to cortical thickness may

reveal biomechanical or developmental patterns that have not been fully explored.

- **Multivariate Demographic Analysis:** Future studies could investigate the relationship between cortical thickness and variables such as ethnicity, diet, geographical location, and socioeconomic status. These factors may influence bone development and density in ways that are currently underexplored.
- **Standardization Across Institutions:** Creating standardized protocols and tools based on this methodology could help unify how bone analysis is conducted across different hospitals and research institutions.

Overall, this work provides a foundation not only for improved medical image analysis but also for advancing personalized medicine and bone health monitoring in pediatric populations. The integration of automation, statistical modeling, and clinical context makes this a promising direction for continued interdisciplinary research.

Annex I: Project alignment with the SDGs

This outlines the explicit alignment of the bachelor's final project, focused on the automated measurement of cortical bone thickness, with three key United Nations Sustainable Development Goals (SDGs) as detailed within the thesis motivation. The work contributes not only to technological innovation but also to broader societal goals related to health, equality, and infrastructure.

SDG 9: Industry, Innovation, and Infrastructure

The project strongly aligns with SDG 9 by contributing directly to research, innovation, and the advancement of medical image processing infrastructure.

- **Contribution to Innovation:** The primary motivation from a research perspective is the development of robust and generalizable tools that require minimal human intervention. By creating and validating an automated algorithm for segmentation and measurement, this project provides an innovative and effective solution to a persistent challenge in medical diagnostics. This aligns with the goal of fostering innovation as a driver of progress and development.
- **Advancement of Medical Technology:** The automation of this analytical process enables large-scale demographic studies of bone development in children, allowing for novel investigations into correlations with age, gender, and other factors. This represents a significant contribution to the technological infrastructure available for medical research.

SDG 3: Good Health and Well-being

The thesis directly addresses SDG 3 by developing a tool designed to enhance clinical practice and provide deeper insights into pediatric bone health. The automated and precise measurement of cortical thickness has numerous beneficial medical applications.

- **Enhanced Disease Monitoring:** The tool can enhance the monitoring of pediatric conditions such as osteosarcoma or osteogenesis imperfecta. It provides a quantitative method for tracking the progression of bone diseases and a patient's response to treatment over time with high precision.

- **Evaluation of Treatment Efficacy:** It can be used to track the efficacy of therapies involving calcium supplementation or other medications designed to improve bone density.
- **Fundamental Research:** The project provides a tool that offers deeper insights into the fundamental processes of bone development during childhood, which is critical for pediatric health.
- **Surgical Planning:** The methodology supports the generation of accurate 3D models of bones, which can aid in the preparation for complex traumatological or orthopedic surgeries.

SDG 10: Reduced Inequalities

The project contributes to reducing inequalities by tackling the economic barriers associated with advanced medical diagnostics.

- **Cost Reduction:** Automating diagnostic processes can significantly reduce the costs associated with clinical judgment by minimizing the hours required for manual analysis by highly trained radiologists.
- **Increased Accessibility:** By making advanced diagnostic technology less expensive, it can become more accessible to a wider population. This helps to ensure that access to high-quality diagnostics is not limited by a patient's geographic location or economic status.

Annex II

Damaged bones discarded from the study:

- Patient 1: 8-year-old female

Figure 1: Unfinished tibia

- Patient 2: 9-year-old male

Figure 2: Porous bone

- Patient 3: 15-year-old female

Figure 3: Abnormal bone

- Patient 4: 36-year-old female

Figure 4: Damaged bone

Unfinished bones: 8-year-old male:

Figure 5: Uncompleted bone

11-year-old female:

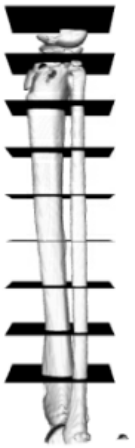

Figure 6: Uncompleted bone

17-year-old male:

Figure 7: Uncompleted bone

Annex III

1. Patient 1: 8-year-old female

2. Patient 2: 9-year-old female

3. Patient 3: 5-year-old male

4. Patient 4: 2-year-old female

5. Patient 5: 9-year-old female

6. Patient 6: 0-year-old male

7. Patient 7: 8-year-old male

8. Patient 8: 8-year-old male

9. Patient 9: 7-year-old male

10. Patient 10: 8-year-old male

11. Patient 11: 11-year-old male

12. Patient 12: 10-year-old female

13. Patient 13: 10-year-old female

14. Patient 14: 10-year-old female

15. Patient 15: 10-year-old male

16. Patient 16: 11-year-old female

17. Patient 17: 11-year-old female

18. Patient 18: 10-year-old female

19. Patient 19: 11-year-old female

20. Patient 20: 11-year-old male

21. Patient 21: 13-year-old male

22. Patient 22: 13-year-old male

23. Patient 23: 13-year-old female

24. Patient 24: 12-year-old female

25. Patient 25: 12-year-old male

26. Patient 26: 12-year-old female

27. Patient 27: 12-year-old male

28. Patient 28: 13-year-old male

29. Patient 29: 13-year-old male

30. Patient 30: 13-year-old male

31. Patient 31: 13-year-old male

32. Patient 32: 12-year-old female

33. Patient 33: 13-year-old female

34. Patient 34: 13-year-old female

35. Patient 35: 14-year-old male

36. Patient 36: 14-year-old female

37. Patient 37: 14-year-old male

38. Patient 38: 15-year-old female

39. Patient 39: 14-year-old male

40. Patient 40: 14-year-old female

41. Patient 41: 14-year-old female

42. Patient 42: 14-year-old female

43. Patient 43: 15-year-old male

44. Patient 44: 14-year-old male

45. Patient 45: 15-year-old male

46. Patient 46: 15-year-old male

47. Patient 47: 15-year-old male

48. Patient 48: 14-year-old male

49. Patient 49: 15-year-old male

50. Patient 50: 16-year-old female

51. Patient 51: 16-year-old female

52. Patient 52: 16-year-old male

53. Patient 53: 16-year-old male

54. Patient 54: 17-year-old male

55. Patient 55: 17-year-old female

56. Patient 56: 17-year-old male

57. Patient 57: 16-year-old male

58. Patient 58: 16-year-old male

59. Patient 59: 17-year-old male

60. Patient 60: 17-year-old male

Bibliography

[1] Alberto Sánchez-Bonaste et al. "Systematic measuring cortical thickness in tibiae for bio-mechanical analysis". In: *Computers in Biology and Medicine* 163 (2023), p. 107123.

[2] Eric H. Chudler. *Brain Slicing: A Primer on Brain Anatomy*. `https://faculty.washington.edu/chudler/slice.html`. Consultado el 20 de julio de 2025. 2023.

[3] Howard Chen. "DICOM Processing and Segmentation in Python". In: *Radiology Data Quest. Np* 28 (2017).

[4] Deependra Rastogi et al. "Deep learning-integrated MRI brain tumor analysis: feature extraction, segmentation, and Survival Prediction using Replicator and volumetric networks". In: *Scientific Reports* 15.1 (2025), p. 1437.

[5] Belén Hernandez Fernandez. *Segmentación de Imágenes Médicas de Huesos Largos Mediante Redes Neuronales*. Trabajo Fin de Grado (Bachelor's Thesis). Madrid, Spain, 2023.

[6] Jiang Hsieh. "Computed tomography: principles, design, artifacts, and recent advances". In: (2003).

[7] Wenjing Du, Jinhuan Zhang, and Jingwen Hu. "A method to determine cortical bone thickness of human femur and tibia using clinical CT scans". In: *2018 IRCOBI conference proceedings, Athens (Greece)*. 2018, pp. 403–412.

[8] Wojtek Rosa. *Advanced DICOM-CT 3D Visualizations with VTK*. `https://example.com/advanced-dicom-ct-3d-visualizations-vtk`. Accessed: 2025-07-02. 2019.

[9] Shingo Ota et al. "Cortical thickness mapping at segmented regions in the distal radius using HR-pQCT". In: *Journal of Bone and Mineral Metabolism* 40.6 (2022), pp. 1021–1032. DOI: `10.1007/s00774-022-01370-2`.

[10] Author(s) Unknown. "Analysis by Synthesis Method for Cortical Bone Modeling from Clinical QCT Scans". In: *[Journal Name]* (2023). Details to be updated once full citation is available.

[11] Valentina Campanelli and Maury L Hull. "Unbiased Method to Determine Articular Cartilage Thickness Using a Three-Dimensional Model Derived from Laser Scanning: Demonstration on the Distal Femur". In: *Bioengineering* 11.11 (2024), p. 1118.

[12] Helen Robson et al. "Interactions between GH, IGF-I, Glucocorticoids, and Thyroid Hormones during Skeletal Growth". In: *Pediatric Research* (2002).

[13] Philip G Murray and Peter E Clayton. "Endocrine Control of Growth". In: *American Journal of Medical Genetics Part C: Seminars in Medical Genetics* (2013).

[14] Arlan L Rosenbloom. "Physiology of growth". In: *Annales Nestlé (English ed.)* 65.3 (2008), pp. 97–108.

[15] BCJ Van der Eerden, Marcel Karperien, and JM14671005 Wit. "Systemic and local regulation of the growth plate". In: *Endocrine reviews* 24.6 (2003), pp. 782–801.

[16] Ola Nilsson et al. "Endocrine regulation of the growth plate". In: *Hormone research in paediatrics* 64.4 (2005), pp. 157–165.

[17] RJ Perry, C Farquharson, and SF Ahmed. "The role of sex steroids in controlling pubertal growth". In: *Clinical endocrinology* 68.1 (2008), pp. 4–15.

[18] Anders Juul. "The effects of oestrogens on linear bone growth". In: *Apmis* 109.S103 (2001), S124–S134.

[19] Yücel Ağırdil. "The growth plate: a physiologic overview". In: *EFORT open reviews* 5.8 (2020), pp. 498–507.

[20] Joyce Emons et al. "Mechanisms of growth plate maturation and epiphyseal fusion". In: *Hormone research in paediatrics* 75.6 (2011), pp. 383–391.

[21] Ja Hyang Cho, Hae Woon Jung, and Kye Shik Shim. "Growth plate closure and therapeutic interventions". In: *Clinical and Experimental Pediatrics* 67.11 (2024), p. 553.

[22] Ola Nilsson et al. "Evidence that estrogen hastens epiphyseal fusion and cessation of longitudinal bone growth by irreversibly depleting the number of resting zone progenitor cells in female rabbits". In: *Endocrinology* 155.8 (2014), pp. 2892–2899.

[23] BC Van der Eerden, Marcel Karperien, and Jan Maarten Wit. "The estrogen receptor in the growth plate: implications for pubertal growth." In: *Journal of Pediatric Endocrinology & Metabolism: JPEM* 14 (2001), pp. 1527–1533.